Gold-Tin Solder Wetting Behavior for Package Lid Seals

Paul T. Vianco, Alice C. Kilgo, and Bonnie M. McKenzie Sandia National Laboratories

P.O. Box 5800 MS0889

Albuquerque, NM 87185-0889

ptvianc@sandia.gov

Abstract

A study examined the cause of non-wetted regions of the gold (Au) finish on iron-nickel (Fe-Ni) alloy lids that seal ceramic packages using the 80Au-20Sn (wt.%, abbreviated Au-Sn) solder and to determine the impact of non-wetting on the final lid-to-ceramic frame solder joint. The Auger Electron Spectroscopy (AES) surface and depth profile techniques identified surface and through-thickness contaminants in the Au metallization layer. The AES surface analysis identified background levels of carbon (C) contamination in vendor-reflowed lids. The depth profile detected C, Fe, and Ni that originated from plating process contamination. Although the C levels were inconsequential, the Fe and Ni could impede the completion of wetting-and-spreading to the edge of the Au metallization. The Au layer of lids not exposed to a Au-Sn solder reflow step, had significant surface and through-thickness C contamination. Inorganic contaminants were absent. Subsequent simulated reflow processes removed the C contamination from the Au layer without driving Ni diffusion from the underlying solderable layer. A Au metallization having negligible surface and in-depth C

concentrations can develop elevated C contamination after exposure to a simulated reflow process due to C compounds originated from the underlying Ni layer. A second reflow step will remove the C compounds from the Au layer. Although the Au metallization showed non-wetted regions, their extent as documented in this study, would not cause them to jeopardize the mechanical strength or hermeticity of the Au-Sn joint.

Introduction

Materials set

Ceramic packages are selected for microprocessors and similar components that support high-reliability electronics systems because they provide a hermetic environment that prevents the active device from being exposed to harsh service conditions. The cover or lid is made from one of several controlled expansion alloys containing iron (Fe), nickel (Ni), and cobalt (Co). These alloys have coefficients of thermal expansion (CTE) that closely match that of the ceramic *frame*, thereby minimizing residual stresses in the lid-to-frame solder joint. Figures 1a and 1b show one such ceramic package. The cross section A-A' is highlighted in Fig. 1c that shows a profile view of the lid assembled to the ceramic frame. The white ovals identify the locations of the lid-to-ceramic solder bond.

The lid is typically attached to the ceramic frame using the high melting temperature, eutectic gold (Au)-tin (Sn) solder alloy, 80Au-20Sn (wt.%, abbreviated Au-Sn). The solidus and liquidus temperatures are 278°C. The high solidus temperature prevents re-melting of the joint when the package is assembled to a printed circuit board using a eutectic tin-lead (Sn-Pb) or Pb-free

solder. Several mechanical properties of the Au-Sn solder were documented by Olsen and Berg [1].

Neither the ceramic frame or lid surfaces are solderable. The lid surface is typically electroplated with a Ni solderable layer followed by a Au protective layer. The recommended layer thicknesses are: Ni, $1.3-3.8~\mu m$ and Au, $1.3-2.5~\mu m$ [2]. In the case of the lid shown in Fig. 1, the entire surface area is electroplated with Ni to prevent general corrosion. Then, masking is used to create a "picture frame" around the perimeter of the lid that is built up with a Ni strike followed by the Au solderable layer. The Au-Sn solder joint is made to this Ni/Au metallization layer.

A different surface finish methodology is used on the ceramic frame. A typical layer stack is shown in Figure 2. The molybdenum (Mo) thick film layer is screen printed around the perimeter of the ceramic frame and fired at high temperatures (900 – 1000°C) to promote its adhesion to the surface. Next, the solderable layer is created by first electroplating a Ni layer on the Mo thick film followed by a Ni/Co alloy layer. Lastly, a layer of Au is electroplated over the Ni/Co layer to preserve the latter's solderability. More details of this ceramic metallization process are provided in reference 3.

Several excellent articles have reviewed the use of the Au-Sn solder in electronic and optoelectronic packages [4-6]. A brief summary is provided here of the interface microstructures. Figure 3a shows the edge of a Fe-Ni alloy lid and the fillet of a Au-Sn solder joint made between the lid and ceramic substrate. The yellow box identifies the location of the

close-up view of the lid/Au-Sn interface shown in Fig. 3b. During the soldering process (which is fluxless), the molten Au-Sn solder wets the Au surface, dissolving the Au layer away, and lastly wets the Ni layer¹. The reaction layer is accompanied by small voids that originated from the volatization of residual organic compounds in the electroplated Au and/or Ni layers. The extent of void formation in this image is typical and would not pose a risk to either the mechanical integrity or hermeticity of the joint.

The reaction layer chemistry can be characterized, qualitatively, by energy dispersive x-ray (EDX) analysis. The SEM image is repeated in Figure 4a. The corresponding x-ray maps are shown for Sn-plus-Ni and Au in Figs. 4b and 4c, respectively. The reaction layer, which is a Au-Ni-Sn intermetallic compound (IMC), has excellent integrity as indicated by the absence of cracking or delamination defects.

The SEM photographs in Fig. 5 show the interface between the Au-Sn solder and the metallization on the ceramic frame. The inset image shows the location of the high magnification SEM photograph. In this case, the Au layer had dissolved into the Au-Sn solder, but had not fully diffused away from the interface, giving rise to the "lobe-like" structures. This behavior is often observed near the fillet toe where the limited volume of molten solder cannot fully dissolve away the Au layer. Nevertheless, the resulting joint exhibits more-than-adequate strength and hermeticity performance.

¹ It is important to reiterate that the Au layer does *not* melt; rather, it is dissolved into the molten solder.

Soldering process

The Au-Sn solder joint is performed without a flux to avoid contaminating the interior volume of the package. In the absence of a flux, wetting-and-spreading by molten Au-Sn alloy is more sensitive to contamination on top of, and within, the Au layer as well as the condition of the Ni layer. Common practice is to use a double reflow process. The first step reflows the Au-Sn solder preform on the lid. By initiating the wetting-and-spreading process, this step provides an indication of the solderability of the Au and Ni layers. The temperature profile also volatizes inorganic contaminants, allowing them to escape from metallization. This procedure is depicted in Figure 6a, which begins with the lid and its Ni/Au metallization (top diagram). The Au-Sn solder preform is tack-welded into place (middle diagram). The assembly is passed through the Au-Sn solder reflow process that melts the preform and allows it to wet and spread over the Ni/Au metallization (bottom diagram).

The second reflow process, which is shown in Fig. 6b, attaches the lid-plus-Au-Sn solder to the ceramic frame. These steps are also performed without a flux. The lid is placed over the ceramic frame (top diagram) and aligned to the metallization. The furnace is evacuated, or filled with the inert gas intended for the internal package volume. The assembly is placed through the Au-Sn reflow process while, at the same time, a downward pressure is maintained between the lid and ceramic frame that forces the molten Au-Sn alloy to spread across the metallization (bottom diagram). The pressure and spreading activity develop a mechanical "agitation" that breaks up the thin Sn oxide on the molten Au-Sn surface as well as allows the molten solder to penetrate the light, organic contaminant layer on the surface of the ceramic frame's Au metallization.

The solderability performance by the (molten) Au-Sn alloy is degraded by excessive contamination of the Au layer surfaces. *Organic contaminants* arise from three sources. First, Au has an affinity to absorb hydrocarbon molecules from the atmosphere. The resulting contaminant layer generally does not affect solderability unless it becomes excessively thick due to prolonged exposure (storage) in heavily polluted environments. The second source is poor plating process control that leads to entrapped plating chemicals in the Au plated layer. Third, inadequate post-plating cleaning processes or poor handling/storage practices can lead to inadvertently surface contamination.

A source of *inorganic contamination* is nickel-oxide (Ni-O) formation on the Au surface. A Ni-O layer develops when Ni diffuses from the solderable layer, through the Au layer, to the latter's surface where it oxidizes upon contact with air. The Ni-O layer is not readily wetted by the molten Au-Sn solder. The extent of Ni diffusion and subsequent oxidation increases with elevated temperature conditions experienced by the metallization prior to the Au-Sn soldering step.

Background for the present study

A lid sealing production process was implemented like that described in Fig. 6. When the steps in Fig. 6a were completed, several locations exhibited incomplete wetting and spreading by the Au-Sn solder on the Au metallization. This condition is shown by the photographs in Fig. 7. Figure 7a shows the entire lid. The yellow box indicates the area viewed at higher magnification in Fig. 7b. The Au layer is exposed because the Au-Sn solder did not spread over it. A concern

was raised that this non-uniform coverage by Au-Sn solder indicates a solderability defect that could lead to Au-Sn solder joints (steps Fig. 6b) having poor mechanical strength and/or lacking hermeticity.

Therefore, a study was performed, the first part of which, was to determine the cause(s) of incomplete wetting-and-spreading by Au-Sn solder (Fig. 7) on the Ni/Au metallization of lids exposed to the steps shown in Fig. 6a. The effort began by using Auger electron spectroscopy (AES) to determine the extent of surface and internal contamination of the Au layer portion of the Ni/Au metallization. This analysis examined test specimens in the as-received condition as well as following simulated reflow cycles. Metallographic cross sections documented the microstructure of the Au-Sn solder on the lid. The second part of the study correlated the contamination condition of the Ni/Au metallization with Au-Sn solderability following the sequence in Fig. 6a, and then with the integrity of the Au-Sn solder joint that resulted from the steps in Fig. 6b.

Experimental procedures

Lid analysis – *previously-reflowed, Au-Sn solder*

The lids were constructed of an Fe-Ni alloy base material, having a thickness of 0.4 mm. Two lids were obtained from the supplier, which already had the 80Au-20Sn (wt.%) solder reflowed on the Ni/Au metallization around the lid perimeter (Fig. 6a). The lids were not exposed to additional cleaning steps. One of the two lids was shown in Fig. 7. Auger electron spectroscopy (AES) *surface surveys* were performed on the exposed Au metallization surface to identify potential contaminant species. Surface surveys were also performed on the Ni electroplated

finish at the interior of the lid as well as on the surface of the reflowed Au-Sn solder. The Au-Sn solder surface included two topographies: the precursor film and the bulk solder. The analyses of the Ni finish and Au-Sn solder benchmarked any generalized contamination of the lid. The experimental error of the AES compositions is ± 0.5 at. % and the sensitivity level is ≥ 1 at.%.

The AES *depth profile* was also performed on the non-wetted Au metallization to determine potential contamination within the electroplated Au layer. After an initial surface survey, the site was sputtered with Ar atoms at intervals of 6 s. Between each six-second interval, an analysis was performed of the elemental concentrations present at that level. The cumulative sputtering time duration was 5 min unless otherwise indicated in the text. In all analyses, the AES depth profiles extended to only within the Au layer. The extensive calibration procedures were not performed to correlate sputtering time to actual depth because they were not required for the objectives of this study.

Upon completion of the AES analysis, the lid in Fig. 7 was then cross sectioned through the Au-Sn solder sessile drop by metallographic techniques to assess the interface microstructure. Scanning electron microscopy (SEM) was used to document the details.

Lid analysis – pristine condition (i.e., those without reflowed Au-Sn solder)

Two lids were obtained from the same supplier that had the Au-Sn solder preform tack welded to the Ni/Au metallization, but were not yet exposed to the initial Au-Sn reflow cycle shown in Fig. 6a. Additional cleaning steps were not performed on the lids. The Au-Sn preforms were carefully removed from the Au metallization. One such lid is shown in Fig 8. Both surface and

depth profile AES analyses were performed on the Au metallization at the four sites labeled A, B, C, and D. These results provided the baseline data set representing the as-received condition.

Next, one lid was exposed to a time-temperature cycle that closely simulated the Au-Sn reflow profile used by the supplier. That profile, which is shown in Fig. 9, had a peak temperature of 308°C and time-above-liquidus (278°C) of ten (10) minutes when performed in the nitrogen atmosphere. The test was performed in a Gleeble® 3500 test system as a batch process. (Gleeble is a trademark of Dynamic Systems, Inc., Poestinkill, NY.) The set-up is shown in Fig. 10. The sample and heater are in a sealed enclosure capable of maintaining either a nitrogen or air atmosphere. Afterwards, the AES analysis was repeated near the same A, B, C, and D locations in Fig. 8.

A second lid was exposed to a reflow profile in the same equipment shown in Fig. 10, but having the nitrogen atmosphere replaced with air. The process profile was slightly hotter and longer than that performed in nitrogen, having a peak temperature of 320°C and time-above-liquidus of fourteen (14) minutes. This test determined the effect, if any, had by the presence of oxygen above the metallization on contamination of the Au layer. Baseline AES data were not obtained from this lid under the assumption that results obtained from the first lid would suitably represent the as-received condition of this second lid. The post-reflow, AES surface survey and depth profile measurements were taken at similar A, B, C, and D locations as depicted in Fig. 8.

Au-Sn solder joint analysis

Three (3) lids were obtained from a second product lot. The *first* lid had the Au-Sn preform removed from it to permit the AES analysis of two sites corresponding to the locations C and D in Fig. 8. These data benchmarked the pristine condition and were assumed to represent the same status for the other two lids. The AES analyses were also performed on the removed Au-Sn preform to establish the presence or absence of general contamination. This first lid was then exposed to a Au-Sn reflow process performed on a conventional belt furnace under a nitrogen atmosphere. The AES, post-reflow analysis was repeated near the same C and D sites.

The *second* lid was passed through the same furnace reflow step, but with the Au-Sn solder preform in place, which allowed it to wet and spread over the Ni/Au metallization. Afterwards, AES surface and depth profile analyses were performed at locations that included non-wetted areas, the precursor film, the surface of the bulk Au-Sn solder (sessile drop), and the Ni metallization at the center of the lid.

The *third* lid, together with the second lid (post-AES analyses) were used to make Au-Sn solder joints to each of two ceramic frames. The ceramic frames had a metallization stack comprised of 4.7±0.6 µm of Au as the protective finish on top of a 5.9±0.8 µm Ni/NiCo solderable layer. The lid-plus-package assemblies were soldered together using the same belt furnace reflow process (nitrogen). The package that used the third lid was subjected to x-ray inspection followed by metallographic cross sections. Non-wetting and void formation, as identified by the radiographs, were correlated to SEM images and EDX analyses of the solder joint microstructure.

Results and discussion

Au and Ni thickness

The thicknesses of the Ni and Au layers were measured from cross sections made to the lid in Fig. 7. Ten (10) measurements were made of the respective thicknesses using SEM images like that in Fig. 11. The Ni and Au thicknesses, which were designated by a mean and an error term of \pm one standard deviation, were 11.6 \pm 0.1 μ m and 1.68 \pm 0.06 μ m, respectively. Cracks and/or delamination defects were not observed in the layers. The Au layer thickness was suitable to protect the solderability of the Ni layer and thereby, support Au-Sn wetting-and-spreading activity.

The Ni thickness was also measured to be 10.3±0.4 µm at the center of the lid. The thickness value was slightly less than that of the Ni/Au metallization because the latter included a strike layer over the pre-existing Ni layer to assure adequate adhesion by the Au layer.

The Au and Ni thicknesses were also measured on one of the three lids used in the Au-Sn solder *joint* study. The Au layer thickness was 2.9±0.1 μm, which is considered *very* thick. Although the Au thickness would not negatively affect Au-Sn wetting-or-spreading (e.g., by constitutional solidification) nor subsequent solder joint performance or reliability, it increases the likelihood of having entrapped organic contaminants from the plating process. The Ni thickness was measured to be 17.9±0.2 μm, which is also *very* thick, being more than is required to support either soldering or corrosion protection functions. Although the cracks and delamination defects were absent from the Ni layer, like a very thick Au layer, it would be more prone to entrapped organic contaminants from the plating bath. The latter scenario will be highlighted in the results, below.

AES: Lids with reflowed Au-Sn solder

The AES surface surveys were performed on the lid that had the Au-Sn solder reflowed at the supplier (Fig. 7). Two locations were selected, which exhibited the non-wetting topography illustrated in Fig. 7b. Those locations were designated "A" and "B" and are shown by the SEM images in Figs. 12a and 12b, respectively.

The AES analysis was performed at four sites per location:

- Site 1, Ni layer that covered the entirety of the lid surface;
- Site 2, the surface of Au layer that was not wetted by the Au-Sn solder;
- Site 3, a precursor film at the edge of the Au-Sn solder; and
- Site 4, on top of the Au-Sn solder "bulk".

The AES surface survey data are presented in Table 1 that were taken at the location A. Although all elemental signals are listed in the table, the sensitivity limit of the AES technique precludes placing a statistical significance on concentrations of less than or equal to 1 at.%. The expected sources of these elements ranged from the air atmosphere (N and S) to plating process contaminants (Ca, P, S, and Cu). Attention was given to the presence of Fe and Co, which were at, or close to, background levels, at all four sites. As contaminants within the Au or Ni layers, Fe and Co would have been subsequently incorporated into the Au-Sn solder (precursor and bulk structures) during the latter's wetting and spreading process. It is not unusual for such trace elements to preferably collect on the molten solder surface oxides.

The discussion examines the elements carbon (C), oxygen (O), nickel (Ni), gold (Au) and tin (Sn) in Table 1. Carbon (C) was present on all surfaces. The predominant source of surface C is hydrocarbons in the air atmosphere. Gold, whether pure (site 2) or as a phase in the Au-Sn solder (sites 3 and 4), is a "getter" for atmospheric hydrocarbons. The typical surface concentration is 30-60 at.%. Therefore, the C concentration levels recorded in Table 1 likely originated from exposure to atmospheric pollution as opposed to an acute source (e.g., handling procedures) or caused by the entrapment of organic plating bath additives. Exposed Ni (site 1), being a less efficient getter, has a lower C concentration on the surface.

The O signal was high at site 1 (18 at. %) in Table 1, which is expected from oxidation of the Ni surface. Oxygen was detected on the Au layer (site 2) at 5 at.%. The most likely source of O at site 2 was oxidation of the traces of Ni, Fe, and Co. A potential source of Ni is diffusion from the underlying Ni solderable finish caused by the time-temperature profile of the Au-Sn soldering process. A second source of Ni, like Fe and Co, is plating bath contaminants that were incorporated into the Au layer. The depth profiles discussed later provide important evidence of the more likely mechanism.

The point is addressed whether the levels of Fe and Ni as oxides, whether on, or within, the Au layer, could degrade Au-Sn solder wetting-and-spreading activity. The authors could not identify a prior study that directly correlated Ni or Fe concentrations with the wetting-and-spreading performance of Au-Sn solder. However, it has been observed that so-called "hard Au" coatings, which include 0.5 - 1.0 wt.% (1.65 - 3.27 at. %) of Co, exhibit less-than-satisfactory

solderability [7]. Therefore, it is possible that Fe and Ni oxides in the Au film are responsible the irregular wetting-and-spreading behavior Au-Sn solder that was the objective of this study.

Elevated O levels were also identified at site 3, the precursor film at the edge of the Au-Sn solder as well as at site 4, on top of the bulk Au-Sn solder. The O concentrations on sites 3 and 4 correspond to the oxidation of Sn-rich phase of the solder that is present at both locations. The higher Au content of the precursor film (site 3) is due to the dissolved Au layer (Fig. 5) as well as any undissolved Au underneath it. The Ni concentrations had dropped to be within experimental error at both sites.

Iron and Co remained present at sites 3 and 4, albeit at, or near to, background levels. The probable sources were contaminants present in the Au and/or Ni layer. Complete and partial dissolution of the Au and Ni layers, respectively, during wetting-and-spreading by the molten Au-Sn solder allowed the Fe and Co atoms to concentrate on the surfaces of both the precursor film and bulk filler metal. Dissolution of the Ni layer would also provide a source of this element at sites 3 and 4 if also present in that layer.

A second location "B" (Fig. 12b) was similarly evaluated by AES. Nearly identical element concentrations and trends were observed; they are listed in Table 2.

An AES surface survey and depth profile were performed within the solid and dashed boxes, respectively, shown by the SEM image in Fig. 13a. This location, which was near that of "A" in

Fig. 12a, targeted a non-wetted Au surface. The higher magnification image in Fig. 13b shows the relatively flat topography that optimizes the fidelity of the AES data.

The surface survey results are shown in the top row of Table 3. Those data were nearly identical to the results in the "site 2, Au layer" rows of Tables 1 and 2. The exception was the elevated O signal of 9 at. % in Table 3 versus 4 - 5 at. % at the other two locations. Because there was not a corresponding increase of Fe, Ni, Co, and Sn that would have oxidized on the surface, the conclusion was drawn that the additional O signal originated from the variant of organic contamination on the Au metallization surface.

The second row in Table 3 was labelled "t=0 Depth Profile Area." Those data originated at the start of the depth profile analysis in the dotted yellow box in Fig. 13b. A small degree of sputtering is performed at the start depth profile sequence, followed by the AES analysis, which establishes time equal to zero ("t=0"). In Table 3, the elemental values were similar to those of the surface survey in the first row. Differences include the loss of the contaminants P, S, and Cl, indicating their presence being limited to only the very surface. As expected, Au increased and C decreased with the removal of organic contaminants on the surface. The additional O signal was attributed to the heightened presence of Ni. The Ni signal is discussed, below. The repeatability of these behaviors was confirmed by a similar analysis performed at the second position near location "B" (Fig. 12b).

The results of the AES depth profile are shown in Fig. 14a for the entire 5 min sputtering sequence. The "surface" of the film is designated at time t = 0 min. The C signal drops off very

rapidly after 10 s, which indicates its source as largely surface contamination. There is the heightened O signal at the surface, a portion of which, was associated with the organic compounds. However, most of the high O level was caused by oxidation of the 3 at. % Ni and 1 at. % Fe present there.

The C, O, Fe and Ni profiles are further analyzed by expanding the sputtering time and concentration axes in Fig. 14b. The reader is reminded that the experimental error on these data is \pm 0.5% and that the sensitivity level is \geq 1 at.%. The Ni and O signals peaked at the surface, and then decreased to background levels (\approx 1at. %) after only a small distance into the Au layer. This Ni had accumulated at the Au surface under an oxidation driving force where it formed a Ni-O compound.

A small Fe peak was also observed just below the surface in Fig. 14b. It is highly unlikely that the Fe originated from the lid base material. Such a scenario was unlikely because it would have required the Fe atoms to diffuse through the Ni layer to reach the Au layer. The more probable source is contamination within the Au layer arising from the plating process. The accumulation of Fe at the surface was driven by an oxidation potential as was also the case of Ni.

Next, the AES analysis moved to the exposed, electroplated Ni finish that covered the lid away from the Au-Sn seal area. A surface survey was performed at one site. A second site was selected for a one-minute, depth profile, which was sufficient to probe into Ni layer beneath any surface oxide or contamination. The elemental concentrations are shown in Table 4, together with the two "site 1" rows duplicated from Tables 1 and 2 (reference, Fig. 12).

The Ni surface exhibited a C concentration of 27%, which was commensurate with levels expected from environmental contamination, and slightly lower than at locations 1 and 2. The one-minute sputtering removed the incidental surface contaminants: N, P, S, Cl, Cu, and Ca. However, O, C, and Co remained at statistically significant concentrations. The persistent O and C signals resulted from organic plating chemicals entrapped in the Ni layer. The source of the Co signal was more elusive. The increased concentration would imply that it is an intentional additive to the Ni layer. However, the absences of Co from energy dispersive x-ray (EDX) analyses of the layer cross sections confirmed that Co was not an intentional additive to the Ni composition; therefore, it was also present as a contaminant from the plating process.

Referring to the presence of Ni in the exposed Au layer (Fig. 14), there are two likely sources:

(a) diffusion from the underlying Ni solderable layer or (b) plating bath contamination. The data in Table 4 indicated a 7 at. % Co concentration in the Ni layer. However, the depth profile in Fig. 14b did not identify Co accompanying the Ni layer. These observations imply that Ni in the Au layer did not diffuse from the underlying solderable layer; rather, its source was a plating bath contaminant.

A metallographic cross section was performed through the Au-Sn solder on the lid. The SEM image in Fig. 15a shows the Au-Sn sessile drop geometry. The high magnification image in Fig. 15b provides a view of the solder/lid interface under the center location of the sessile drop. The voids formed by the volatization of organic compounds that originated from the electroplated Au and/or Ni layers. The voids had their greatest concentration at the center location where there is

complete dissolution of the Au layer and the greatest extent of Ni dissolution. The concentration of voids would be considered as "low" for this application.

The SEM image in Fig. 15c shows the edge of the sessile drop. Obvious contamination or other anomalies were not evident in the Au or Ni layers. The small contact angle, θ_c , indicated that the Au-Sn solder exhibited very good solderability on the Au layer. However, the solder did not spread over the distance X-Y. It is hypothesized that the reduced driving force for wetting-and-spreading could not overcome the effects of Ni and Fe oxides on the Au surface.

In summary, the AES analysis determined that *surface* C contamination of the Au and Ni layers was commensurate with the gettering of environmental hydrocarbons (air pollution) and would not, in-and-of-itself, lead to solderability degradation. Also, C contamination *within* the Au film originated from the plating process. Those concentrations were also unlikely to affect Au-Sn solderability. Iron and Ni were observed in the Au layer, which were introduced by the plating process. These contaminants could potentially impede full coverage of the Au metallization, particularly near the edge of the metallization, where the driving force is reduced for the final stages of wetting-and-spreading activity.

AES: Pristine lids

The AES analysis was performed on a lid that had *not* been previously exposed to the Au-Sn solder reflow cycle at the supplier. The Au-Sn solder preform was removed from the Au metallization. Surface surveys and depth profiles were taken at the four sites A, B, C, and D

shown in Fig. 16 to establish the baseline data. Note that depth profile data, which were obtained at sites C and D, were done so for one- and two-minute durations, only.

The AES surface survey results are shown in Table 5. The C concentrations are nearly identical for the four sites. The values were commensurate with environmental organic contaminants gettered by the Au surface. Besides C, both Ni and Cu were detected at location A, but having values that were at and below background levels, respectively.

Depth profiles were performed at the four locations. The Ni and Cu signals disappeared at location A after 0.1 min of sputtering, implying that they were minor contaminants from the plating process and signaled a lot-to-lot variation of these elements. The C (blue) and Au (red) profiles are shown in Fig. 17 for locations A and B, which are also representative of the C and D locations. The C signal decreased and the Au concentration increased with depth (sputtering time) into the film. But, the C concentration did not reach zero; rather, it leveled off to a value of approximately 6%. This sustained C signal is a result of organic compounds that had become entrapped in the Au layer during the plating process.

The C signal exhibited dissimilar trends between Figs. 17 and 14. There are two possible scenarios. The first scenario has that difference being caused by simply a lot-to-lot variation of organic compounds entrapped in the Au layer during the plating process. The second scenario proposes that C contamination was the same between the two lids in the pristine condition. However, the reflow process (at the vendor) caused volatization of those organic compounds, resulting in the absence of C in the Au layer analyzed in Fig. 14. It is not possible to confirm the

first scenario because lids were not available from the earlier lot that were not exposed to the reflow process. The viability of the second scenario, however, can be assessed with further data obtained in the next section.

Lastly, the residual C levels observed in Fig. 17 are unlikely to significantly degrade the solderability of the Au layer by molten Au-Sn solder. Rather, the predominant consequence is additional void formation in the Au-Sn solder after the reflow step in Fig. 6a.

AES of pristine lids exposed to the simulated reflow profile

The lid used to analyze the "as-received" condition (Fig. 17) was subsequently exposed to the simulated reflow process using the equipment shown in Fig. 10. The reflow was performed in the nitrogen environment. The resulting AES depth profiles are shown in Fig. 18 for the C and Au concentrations at all four locations. The surface concentrations of C were in the range of 39 – 49 at. %, which is slightly higher than the 30 – 35 at. % observed for as-received condition (Fig. 17). However, unlike the data in Fig. 17, the C levels dropped rapidly to zero between sputtering times of 0.5 and 1.0 min. The slightly elevated surface C levels, together with the absence of significant C measured in the depth profile, indicated that the reflow step volatized the organic compounds from the Au layer.

Nickel was not detected in Fig. 18 following the reflow event. Prior to reflow, a trace Ni was present as a plating bath contaminant at one location. The general absence of Ni confirmed that the reflow process did not drive Ni diffusion into the Au layer from the solderable layer underneath it. Therefore, the presence of Ni (and Fe) in Fig. 14 (post-vendor reflow, non-wetted

Au surface) is indicative of a lot-to-lot variation of these contaminants to be expected from the plating process.

Measurable concentrations were detected of silicon (Si) and O. Those profiles are shown in Fig. 19. At the surface, the Si and O concentrations were in the range of 3 – 9 at. % and 3 – 13 at. %, respectively. These elements were limited to the immediate surface of the Au layer given their rapid decrease to zero after the very short etching times. In the absence of other elements, it was concluded that the O signal was associated with oxidation of Si. The likely source of Si and O was cross contamination from apparatus heating stage.

The AES analysis was also performed on a second pristine lid that was exposed to the same simulated Au-Sn reflow profile, but in an *air environment*. This lid did not have either surface or depth profiles performed prior to the reflow exposure under the assumption that it was suitably represented by the data in Fig. 17. The C and Au depth profiles are shown in Fig. 20 for the four locations A, B, C, and D. Surface C concentrations were 25 - 60 at. %, which varied more than after the nitrogen reflow (Fig. 18), but on average, were commensurate with the latter case. The C profiles rapidly dropped to zero after 0.5 - 1.0 min of sputtering as was also observed in Fig. 18. These data indicate that C surface and depth profiles were not sensitive to the nitrogen versus air environment above the metallization.

The Ni, Fe, and Cu signals were zero at all but one the location (B) after the air reflow step. At location B, a Ni concentration was recorded at 7 at. %; however, it rapidly dropped to zero after

only 0.1 min of sputtering. Therefore, the Ni was present as a plating process contaminant and did not originate by diffusion from the underlying solderable layer.

The Si and O signals were also observed on the Au surface after the air reflow process. The concentrations were slightly greater than those observed in Fig. 19. However, they also decreased to zero after the 0.5 min sputtering time, thereby substantiating the earlier conclusion that Si was a contaminant that originated from the heating apparatus.

Lid-to-package assembly process – AES surface and depth profile analyses

The objective of the next analysis was to correlate the level of contamination on, or within, the Au layer to the integrity of the Au-Sn solder joint made between the lid and a ceramic frame.

Three lids were used in this effort, which had not had the Au-Sn preform reflowed to the metallization by the process in Fig. 6a.

This study began by establishing baseline AES surface surveys and depth profiles of the Au layer. The data, which were obtained from one lid, were assumed to also represent the other two parts. The Au-Sn preform was removed from the Ni/Au layer. The AES analyses were performed at two locations similar to C and D in Fig. 8. Unlike the previous assessments, the AES depth profiles were extended to fifteen (15) minutes. The AES data were obtained only from Au layer.

The AES profile is shown in Fig. 21 for C and Au signals. The C concentration at the surface was 20 - 35 at. %, which is expected from contamination by environmental hydrocarbons. The

C signal rapidly dropped to zero after 0.1 min of sputtering, and remained at that level for the rest of the sputtering time. Nickel and Fe were not detected over the entire fifteen-minute sputtering interval.

The same analysis was performed on the Au metallization layer belonging to the ceramic package. The AES surface data showed C surface concentrations of 65 at. % and 77 at. %, which are nearly twice the levels observed on the lid, but still commensurate with the gettering of hydrocarbons from the atmosphere. The C signals dropped rapidly to zero after sputtering for 0.1 min. No other elements were detected in depth analysis.

The AES surface and depth profiles were performed on the Au-Sn solder preform. Excessive surface C contamination and/or thick Sn oxides can impede the initial wetting-and-spreading step depicted in Fig. 6a. Reflow temperatures are generally too low to significantly reduce the surface oxides. Identical AES surface and depth profiles were obtained at two locations on the Au-Sn preform, one of which is plotted in Fig. 22. Only C, Au, Sn, and O were detected in the AES analysis. The C signal at the surface was 38 at. % and caused by the gettering behavior of the Au-rich phase. The O signal of 29 at. % resulted from oxidation of the Sn-rich phase. The C signal was reduced to zero after 0.1 min of sputtering and the O signal disappeared after sputtering for one minute. Both behaviors confirmed that the C contamination and oxide were present as only thin surface layers. Further sputtering resulted in a depth profile representing the Au-Sn solder composition.

The lid, from which was taken the AES depth profile of the Au metallization shown in Fig. 21, was exposed to the Au-Sn, *belt furnace* reflow profile (nitrogen). The follow-up, AES depth profile is shown in Fig. 23 for the C and Au signals. Those data were compared to the depth profile in Fig. 21 (as-received). The C signal rapidly dropped at location C after 0.1 min of sputtering, but not to zero; rather, it remained a 3 at.%. The location D site had a greater accumulation of C contamination near the surface, requiring two minutes of sputtering to reach the same 3 at. % level. The C concentrations remained at 3 at. % at both locations for up to eight minutes of sputtering before dropping to zero. The C signals remained at zero for the remainder of the depth profile.

The trend observed in Fig. 23 was unexpected, given that Fig. 21 indicated an absence of C beyond the immediate surface (sputtering time ≥ 0.1 min). The reflow process was expected to remove organic contaminants from a layer as was observed when comparing Fig. 17 (asreceived) to Fig.18 (post-reflow). In effect, Fig. 23 implies that the reflow profile *increased* C contamination into the Au layer.

The different trends were attributed to the different starting levels of C in the Au layer. The lid exemplified by Fig. 17 started out with a very high C concentration. Exposure to the reflow conditions removed those contaminants as shown by Fig. 18. On the other hand, the lid represented by the AES profile in Fig. 21 started out with very low levels of C contamination throughout the Au layer thickness. The reflow conditions caused organic contaminants to accumulate within the Au layer and more so at the surface as observed in Fig. 23.

An analysis was made to identify the source of the organic contaminants. Although C contaminants can accumulate on the Au surface from the environment, their large molecular size would hinder diffusion very far into the Au layer thickness, certainly not to the degree observed in Fig. 23. Rather, the hypothesis was considered that the *Ni layer* was the source of organic contaminants. The post-one-minute sputtering results in Table 4 identified a 6 at. % C concentration within the Ni layer for the as-received condition. An AES depth profile was then performed on the Ni layer towards the center of the present lid *after exposure to the reflow cycle*. Those data are shown in Fig. 24. The C concentration was 10 at. % after one minute of sputtering, which is even higher than that observed in Table 4. The O level reduced to 1 at. % after ten minutes of sputtering into the Ni layer. The data in Table 4 and Fig. 24 confirmed that the Ni layer was a potential source C contamination. Moreover, the organic contaminants in the Ni layer, which are entrapped from the plating bath, can diffuse within the film and into the Au layer under the elevated temperatures of the reflow profile.

The Au layer exhibited Ni and Si signals that were within the measurement error (≤ 1 at. %) after exposure to the reflow cycle. The negligible Ni signal confirms the absence of its diffusion from the solderable layer into the Au layer. The belt furnace did not introduce Si contamination on the surface. Sodium (3 at.%) and S (2 at.%) were observed on the surface at the D location, but were absent from location C, which suggests their sources being *incidental* contamination from the environment or the plating process.

A second lid was exposed to the belt furnace reflow process. In this case, the Au-Sn solder preform remained in place and allowed to wet and spread over the Au metallization by the

process described in Fig. 6a. A stereo photograph of the lid is shown in Fig. 25a. Numerous areas of non-wetting were observed on the Au layer. The AES analysis targeted locations A and B that are shown in Figs. 25b and 25c, respectively, as well as the nearby precursor film and bulk Au-Sn solder. Data were obtained from the exposed Ni plating layer at location C. In the latter case, three separate measurements were made at the site; the results were presented as an average of those analyses.

The AES depth profile is shown in Fig. 26 that was taken of the *non-wetted Au layer* at location A shown in Fig. 25b. The depth profile was identical at Location B. The C concentration was 70 at.% at the surface, which is relatively high vis-à-vis the getting mechanism. More importantly, the C signal remained elevated throughout the thickness of the Au layer, decreasing from 70 at.% at the surface to 20 at.% after one minute, where it remained through four minutes of sputtering. After four minutes, the C concentration gradually decreased, reaching a still high value of 12 at.% following ten minutes of sputtering activity.

The trend in Fig. 26 was consistent, qualitatively, with the behavior of the first lid. Assuming that the as-received AES profile in Fig. 21 represented this second lid, both samples experienced an increase of C contamination at the surface and near-surface volume of the Au layer following exposure to the reflow cycle (Fig. 23). The magnitude of the effect was greater in the case of the second lid (Fig. 26). The same mechanism is proposed to explain the trend in Fig. 26 – that is, C diffused from the Ni layer into the relatively "C-free," Au layer upon exposure to the reflow profile.

The AES depth profile in Fig. 26 is compared to that in Fig. 14, which originated from the non-wetted Au layer of a lid reflowed at the supplier. Both plots showed traces of Sn that were near the detection limit. The significant differences between the two cases were (a) the absence of the Ni and Fe contamination and (b) the sustained C contamination observed in Fig. 26 profile, but were absent from Fig. 14. Although viable scenarios have been presented for both phenomena, these differences confirm the condition of the Au layer has a lot-to-lot variation that reflects upon the control of the plating process.

Intrinsically, a more important conclusion was drawn from the comparison of Figs. 26 and 14. Recall that the presence of Ni- and Fe-oxide in the near-surface Au layer as shown in Fig. 14, was considered to be a potential cause for incomplete spreading of the Au-Sn solder over the Ni/Au metallization. The current experiment shows the same incomplete wetting (Fig. 25), but without the Ni and Fe contamination. The conclusion was drawn that the elevated C contamination of the Au layer hindered the final stages of wetting-and-spreading by molten Au-Sn solder towards the edge of the Au metallization.

The precursor film sites were examined at locations A and B in Fig. 25. The AES depth profile is shown in Fig. 27 for location A. The location B profile differed only slightly due to variations in the extent of Au dissolution under the precursor layer. The C signal was 58 at.% at the surface. The surface O signal, which was attributed to the exposed Sn-rich phase of the solder, was removed after one minute of sputtering. These surface survey results generally matched those provided in Tables 1 and 3 for the same precursor films generated by the supplier reflow cycle.

The interesting feature of Fig. 27 was the C signal. The C level dropped from 58 at.% to 6 at.% after only 0.1 minutes of sputtering activity, and then increased to 10 at.% where it remained for all but the last two minutes of the ten-minute sputtering duration. This trend indicates that the elevated C contamination within the Au layer (Fig. 26) was incorporated into the precursor layer of the advancing Au-Sn solder as the latter dissolved the Au layer into it. The contamination had not yet volatized from the Au layer.

The results of the AES surface and depth profile analyses are shown in Fig. 28 for the bulk Au-Sn solder. In this case, location B provided the data. The data corroborated the surface survey data shown in Tables 1 and 2 for the same locations. The depth profile of Fig. 28 was compared to that in Fig. 22, which was obtained from the surface of the non-reflowed, Au-Sn preform. Both plots show the same presence of Sn and O as Sn-O, as well as C at the surface. A marked difference was that both the C and O signals remained elevated in Fig. 28 throughout the tenminute sputtering duration. It was concluded that the elevated C concentration in the precursor layer (Fig. 27) was subsequently incorporated into the bulk Au-Sn solder.

The above analysis indicates that contaminants are not entirely volatized from the Au layer by the Au-Sn soldering process (Fig. 6b). It was surmised that, in this particular instance, the C contamination was introduced into the Au layer from the Ni layer. Subsequently, the C contamination became incorporated into the precursor film and bulk molten Au-Sn solder. This result implies that removal of C contaminants should be maximized in the Fig. 6a process.

Otherwise, the volatization of such contaminants becomes reduced by the wetting-and-spreading of the molten Au-Sn solder in the Fig. 6b process

Lid-to-package assembly process – Au-Sn solder joint x-ray and cross section analysis

The second and third lids was used to determine the effect of organic contaminants on the formation of the Au-Sn solder joint between the lid and ceramic frame. The third lid had the Au-Sn solder preform reflowed per the process in Fig. 6a. Then, it along with the second lid were attached to the ceramic frame using the steps in Fig. 6b. The third lid was assumed to be in the same as-received condition as the first lid (Fig. 21) as well as reflect the condition of the second lid after the reflow step in Fig. 6a (Fig. 26). A visual inspection did not identify any defects in the completed lid-to-ceramic frame joint.

Similar data were obtained from both assemblies; the package having the third lid will be highlighted in the following discussion. X-ray images of the entire joint footprint showed an absence of significant void formation from around the solder joint gap as well as the fillet. A representative x-ray is shown in Fig. 29a that illustrates this observation. The white arrow indicates the solder joint gap and the black arrow, the fillet. This image also shows the only length of bond from around the perimeter in which the Au-Sn solder did not spread fully to the edge of the Au metallization on the lid. That region is indicated by the white bracket. The fact that similar areas were *not* observed elsewhere implies that the non-wetting was caused by a local change in solderability of the Au metallization (lid) rather than an inadequate supply of filler metal. The length of joint in the yellow box is shown at higher magnification in Fig. 29b.

The loss of wetted area would certainly not impact either the mechanical strength or hermeticity functions of the solder joint.

The x-ray images in Fig. 29 also indicate that the C contamination present in the lid's Au metallization did not result in excessive void development in the joint. Volatization of the C contamination occurred from the Au metallization during the Au-Sn soldering process. Then, the pressure applied between the lid and ceramic frame (Fig. 6b) forced any voids from the gap. This scenario corroborates the AES depth profile data in Figs. 17 and 18, which show that the reflow cycle can remove a sufficient degree of organic contaminants from the Au layer. The absence of voids suggests that the volatization of contaminants occurred prior to wetting-and-spreading by the molten Au-Sn solder.

Metallographic cross sections were made of Au-Sn solder joint on the third lid. The locations of those cross sections are shown in Fig. 30. Sections 1 and 4, which intercepted the full length of the Au-Sn solder joint, confirmed the excellent integrity of the entire bond length. Only a few, isolated voids were observed in the solder.

The sections 2 and 3 provided views of the solder joint width at the non-wetted regions identified in Fig. 29. Figure 31 shows a series of increasingly higher magnification, SEM images of section 2 where the Au-Sn solder wet and spread over the entire width of Au metallization on the lid. The low magnification image at top confirmed filling of the gap and formation of a suitable fillet along the edge of the lid (magenta arrow). The lower left-hand photograph shows that the Au-Sn solder had wet and spread to the edge of the Au metallization on the lid. Since the region

in the yellow box was removed from the gap, wetting was not assisted, expressly, by the pressure applied between the lid and ceramic frame. The lower right-hand SEM photograph confirmed the absence of both constitutional solidification and dewetting by the thin Au-Sn solder film.

Similar sets of SEM photographs are provided in Figs. 32 and 33, which were taken on the other side of the package at section 2 and section 3, respectively. The cross sections targeted the behavior of incomplete coverage of the lid's Au metallization that occurred along the joint perimeter identified in Fig. 29. In both Figs. 32 and 33, the top photograph confirmed overall good solderability of the lid and ceramic frame. The lower left-hand SEM photographs show the non-wetted stretch of Au metallization on the lid. The Au-Sn solder profile differed between Figs. 32 and 33 due to different extents of spreading on the Au metallization.

The lower right-hand images of Figs. 32 and 33 show that the different fillet profiles have relatively low contact angles (θ_c), thereby confirming the overall good solderability of the Au metallization up to the stopping point. There, the slightly degraded solderability prevented final coverage of the metallization layer by the molten Au-Sn solder under a reduced driving force caused by the transition from capillary flow to that of surface wetting-and-spreading by the sessile drop geometry. Contributing to the loss of driving force in the latter case was the absence of the benefit provided by the applied pressure.

The analysis continued by combining the AES data with these microstructural results of the lid-to-ceramic frame solder joint. Persistently high, C contamination were inferred in the Au layer of the third lid after the first reflow process (Fig. 6a), based upon the AES data taken of the first

two lids after the same step; see Figs. 23 and 26. Nevertheless, catastrophic defects such as large-scale poor solderability or excessive voids were not observed in the final lid-to-ceramic frame solder joint. That is, the non-wetted Au surface areas shown in Fig 25 did *not* predict a poor solder joint after the lid-to-frame assembly process. The radiographs and SEM images confirmed an absence of significant void development, indicating that contaminants still present in the Au layer do not necessarily undergo a volatization event that creates such voids in the joint.

In summary, the present study determined that there can be two systemic sources of contamination with respect to the Au layer on the lid². The first source, which includes both organic as well as inorganic contaminants, is the Au plating process. The second source of primarily organic contaminants, is their diffusion from the Ni layer into the Au layer upon exposure to temperatures commensurate with a reflow cycle. The initial reflow step (Fig. 6a) can benefit the final package solder joint under the first scenario because it removes organic contaminants that are already in the Au layer. Under the second scenario, the first reflow step drives organic contaminants from the Ni layer into the Au metallization. However, it appears that the second reflow step removes them from the Au layer, but in a manner that does not necessarily generate significant voids in the lid-to-ceramic frame solder joint. Inorganic elements, which are incorporated into the Au layer by the plating process, are unlikely to be volatized from the metallization layer. Rather, they are more likely to concentration at, or near to, the surface and pose a greater risk to solderability of the Au metallization layer. Both

² Of course, there are acute sources of surface contamination – handling mishaps, storage in an excessive polluted environment, etc., which are not considered in this discussion.

contaminant species impeded final wetting-and-spreading, but only did so, here, in terms of final coverage to the edge of the Au metallization. That level of non-wetting would not impact the mechanical strength or hermeticity of the joint. Lastly, neither one or two exposures to the reflow conditions caused Ni diffusion from the solderable layer and into the Au metallization to a degree that was detected by the AES depth profiles.

Summary

- 1. A study was conducted to identify the cause of non-wetted regions of the gold (Au) finish on Fe-Ni alloy lids used to seal ceramic packages by means of the 80Au-20Sn (wt.%, abbreviated Au-Sn) solder. A concurrent objective was to determine the impact of the non-wetting phenomenon on the final lid-to-ceramic frame solder joint. The Auger Electron Spectroscopy (AES) surface and depth profile techniques were used to identify surface and through-thickness contaminant species in the Au metallization layer.
- 2. A lid was examined that exhibited the non-wetted Au surface behavior. The AES surface analysis identified carbon (C) contamination, but to a level commensurate with the gettering behavior of Au surfaces. The depth profile detected C, iron (Fe), and nickel (Ni) in the Au layer that originated from plating process contamination. Although the C levels were inconsequential to Au-Sn wetting-and-spreading, the Fe and Ni contaminants could impede Au-Sn solderability, especially near the edge of the Au metallization.
- 3. The Au layer on lids, which had not been exposed to the initial Au-Sn solder reflow step, had significant surface and through-thickness C contamination. Inorganic contaminants were absent. Subsequent simulated reflow processes, whether performed under a

- nitrogen or air environment, removed the C contamination from the Au layer without driving Ni diffusion from the underlying, Ni solderable layer.
- 4. A lid, which came from another product lot, showed only a nominal surface C signal and negligible C in the depth profile. However, after exposure to a simulated Au-Sn reflow process, the AES analysis detected elevated surface and through-thickness C contamination at non-wetted Au metallization areas. These C contamination levels impeded the later stages of Au-Sn wetting-and-spreading to the edges of the Au metallization edge. The contamination originated from the underlying Ni layer.
- 5. The second reflow step, which creates the final lid-to-ceramic frame Au-Sn solder joint, can remove C contamination. In the present study, it did so without the volatization event that creates significant void formation. Although non-wetted regions were observed at the edge of the lid's Au metallization layer, their extent did not jeopardize the mechanical strength or hermeticity of the final lid-to-frame Au-Sn joint.

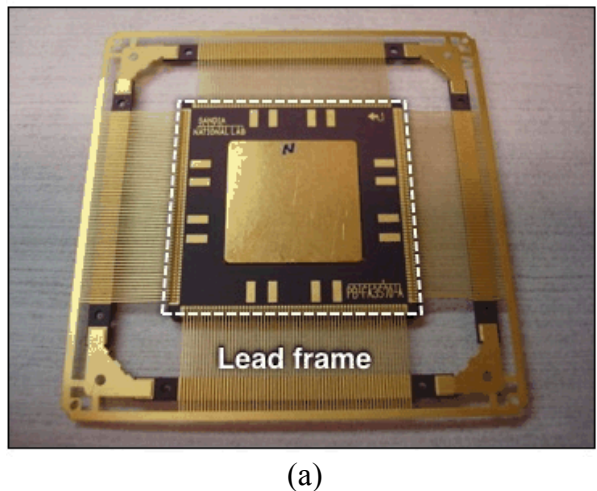
Acknowledgements

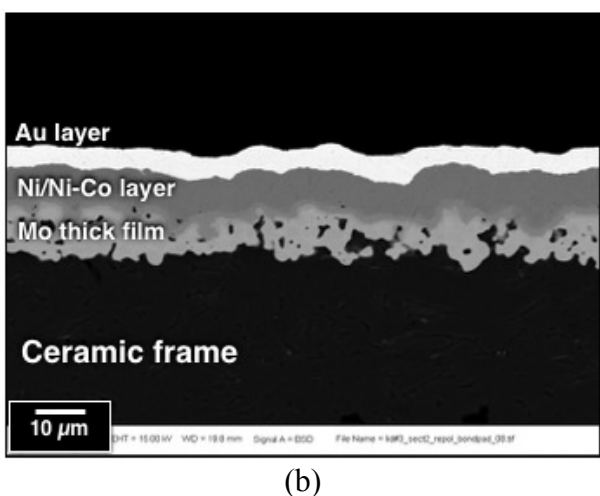
The authors wish to thank Zahra Ghanbari for her thorough review of the manuscript. Sandia National Laboratories is a multi-mission laboratory managed and operated by National Technology and Engineering Solutions of Sandia LLC, a wholly owned subsidiary of Honeywell International Inc. for the U.S. Department of Energy's National Nuclear Security Administration under contract DE-NA0003525.

References

- [1] Olsen, D. and Berg, H., 1979, "Properties of Die Bond Alloys Relating to Thermal Fatigue," IEEE Trans. Comp. Hybrids, and Manuf. Tech., CHMT-2, pp. 257-263.
- [2] Vianco, P., 1998, "An Overview of Surface Finishes and Their Role in Printed Circuit Board Solderability and Solder Joint Performance," Circuit World, 25, pp. 6-24.
- [3] Holmes, P. and Loasby, R., 1976, *Handbook of Thick Film Tec*hnology Electrochem Pub. Ayr, Scotland, pp. 189 191.
- [4] Matijasevic, G., Lee, C., and Wang, C., 1993, "AuSn Alloy Phase Diagram and Properties Related to its Use as a Bonding Medium," Thin Solid Films, 223, pp. 276-287.
- [5] Oppermann, H., 2005, "The Role of Au/Sn Solder in Packaging," *Materials for Information Technology*, E. Zshech, C. Whelan, and T. Mikolajick, eds., Spinger, London, England, pp. 377-390.
- [6] Ivey, D., 1998, "Microstructural Characterization of Au/Sn Solder for Packaging in Optoelectronic Applications," Micron, 29, pp. 281-287.
- [7] Christie, I. and Cameron, B., 1994, "Gold Electrodeposition Within the Electronics Industry," Gold Bulletin 27, pp. 12-20.

Figure Captions





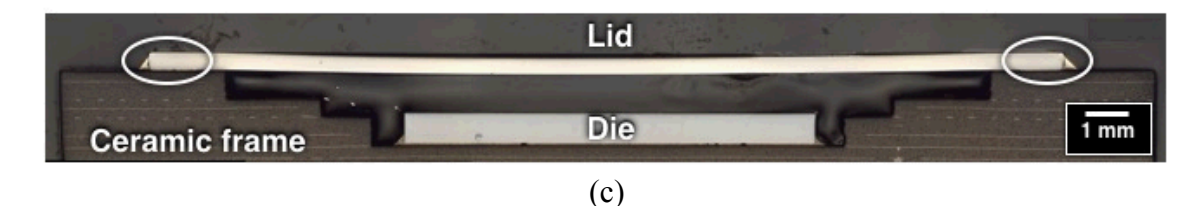


Fig. 1 (a) Photograph shows a ceramic package in its lead frame. (b) Top-down view outlines the ceramic frame, lid, and the leads. (c) The cross section A-A' shows a profile view of the lid attached to the ceramic frame. The white ovals identify the location of the lid-to-ceramic solder bond.

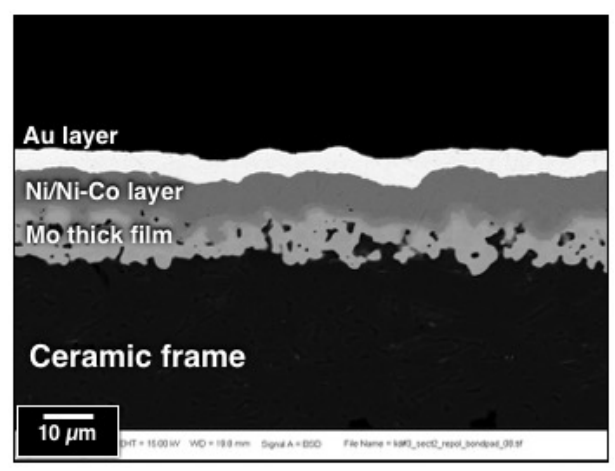
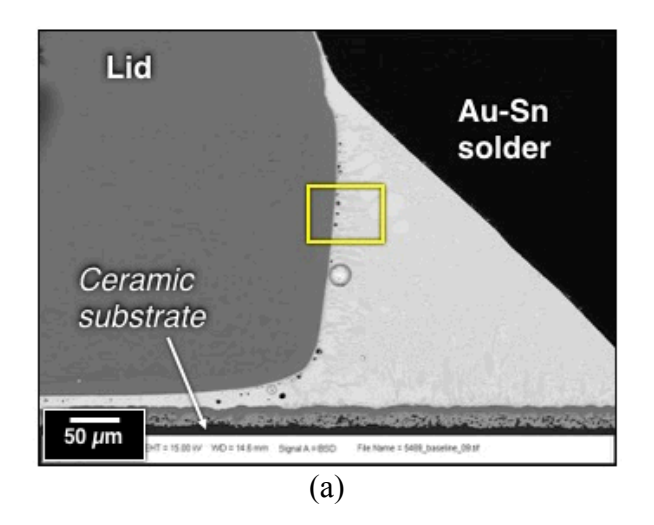


Fig. 2 SEM photograph shows the metallization layer on the ceramic frame (substrate): Mo thick film adhesion layer, Ni/Ni-Co solderable layer, and the Au protective layer.



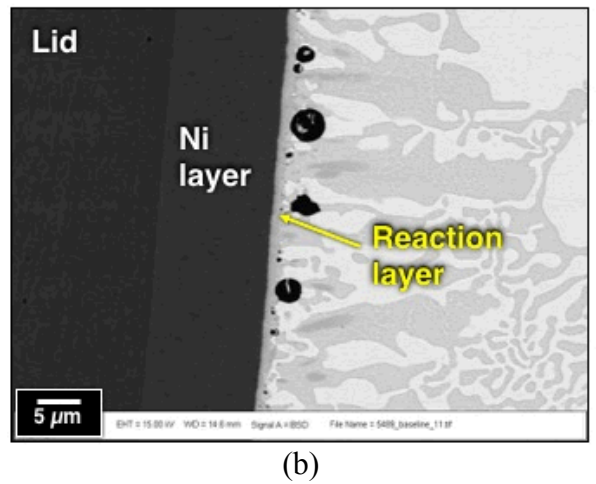
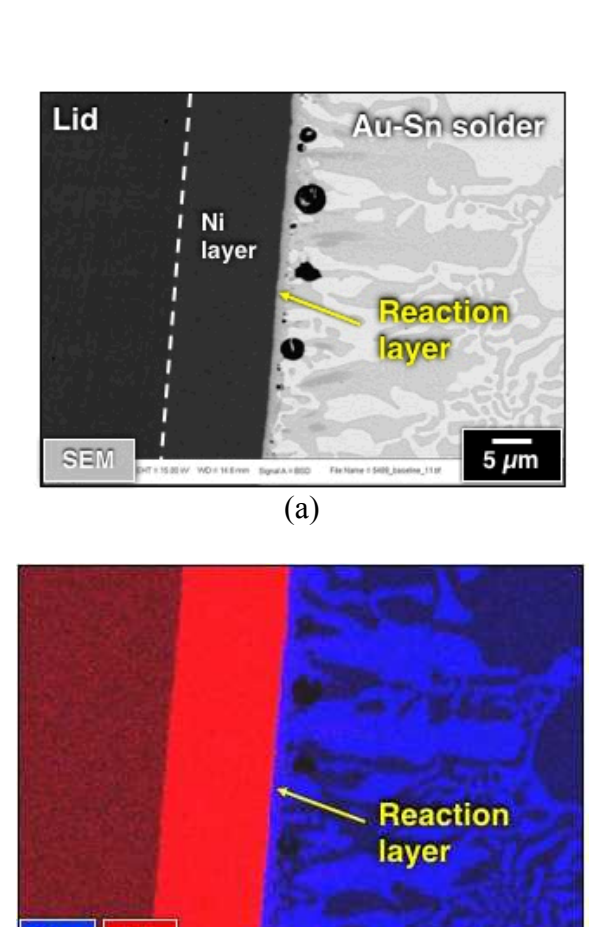
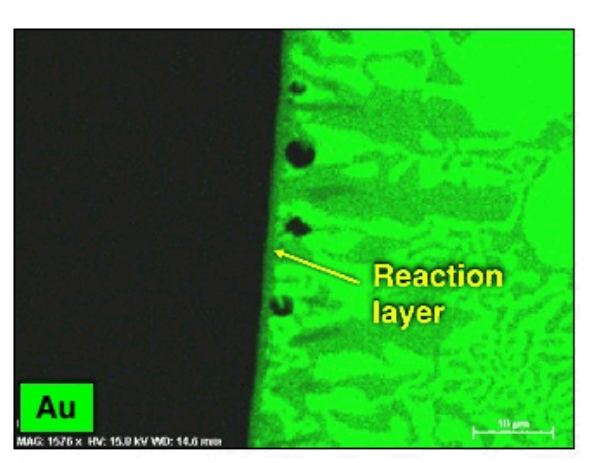


Fig. 3 (a) SEM photograph shows the fillet of a Au-Sn solder joint made to the Ni-plated, Kovar™ lid and ceramic substrate. (b) Higher magnification image was taken of the lid (Ni layer)/Au-Sn solder interface. A reaction layer, which formed along the interface, was accompanied by intermittent voids.





(b)

Fig. 4 (a) SEM image shows the lid (Ni layer)/Au-Sn solder interface. (b, c) EDX maps show the area distributions of Ni together with Sn as well as that of Au.

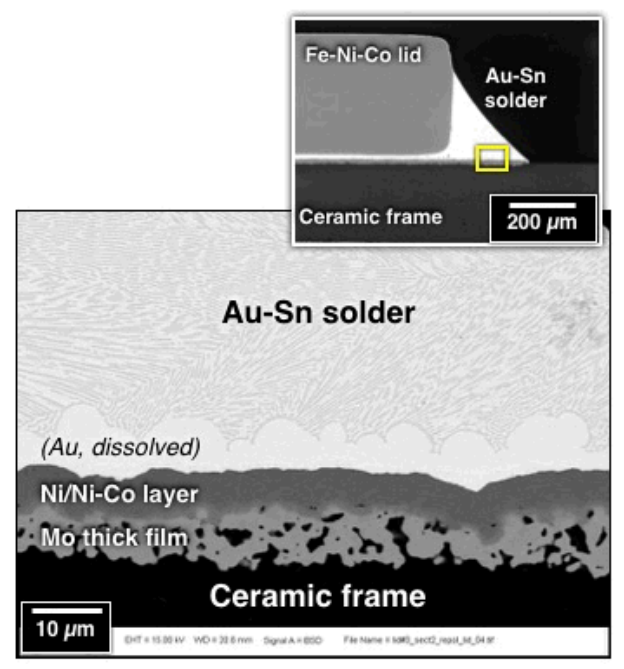


Fig. 5 SEM image shows the interface between the ceramic frame's metallization and the Au-Sn solder at the location indicated by the yellow rectangle in the inset photograph. The Au had not yet fully dissolved into the volume of molten Au-Sn solder.

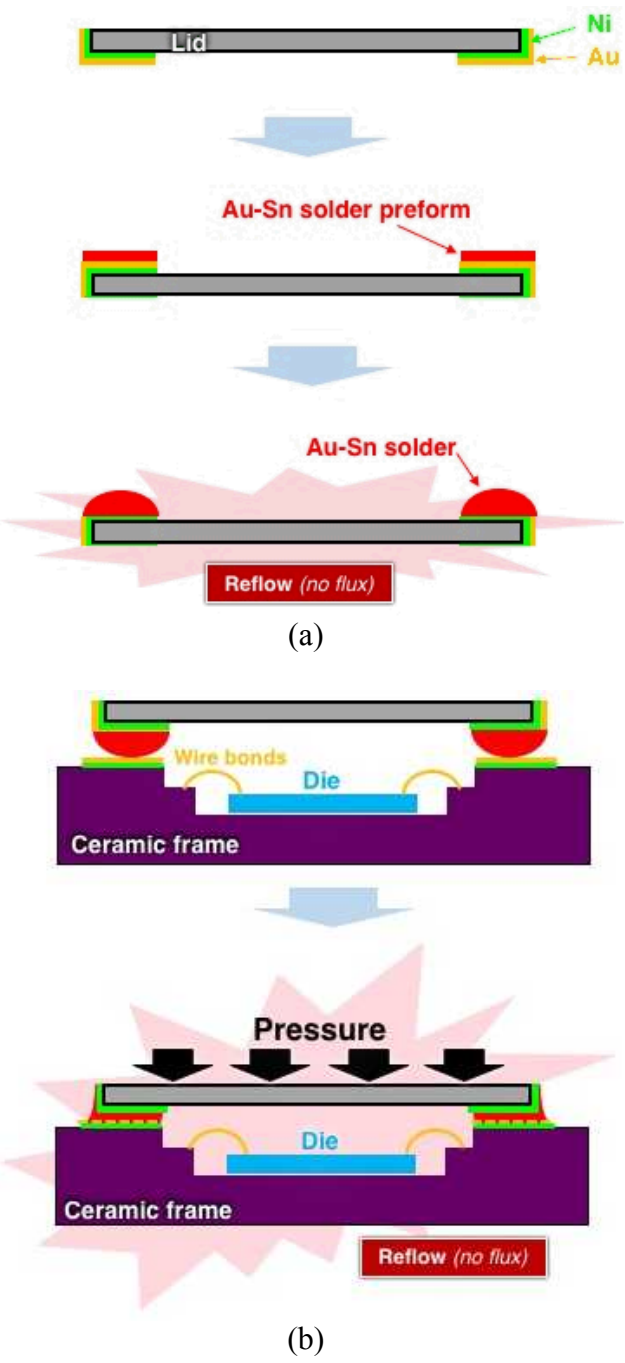
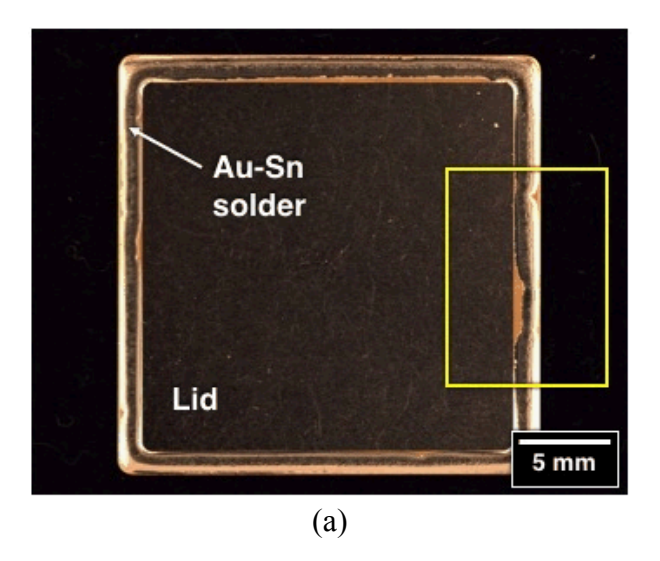


Fig. 6 Schematic diagrams show the double reflow procedure used to fabricate the Au-Sn lid (seal) solder joint. (a) The lid is fabricated with the Ni/Au metallization (top). The Au-Sn solder is tack welded on the Ni/Au metallization (middle). The reflow step allows wetting and spreading of the molten Au-Sn solder (bottom). (b) The lid-plus-Au-Sn solder assembly is aligned to the ceramic frame metallization (top). Pressure is applied to the lid during the reflow step to promote wetting and spreading activity by the molten Au-Sn solder to complete the joint (bottom).



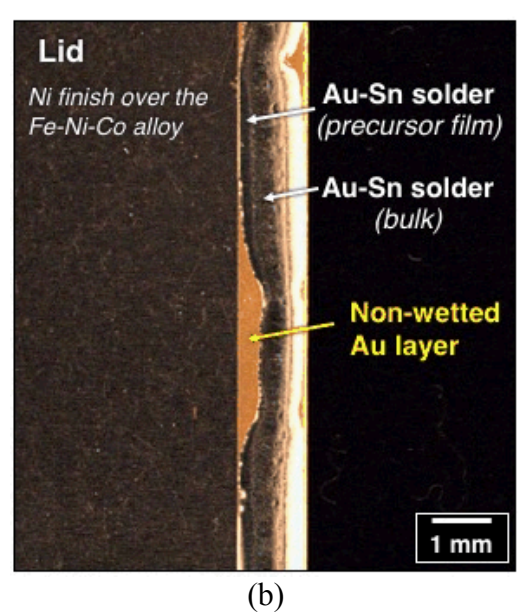


Fig. 7 (a) Photograph shows a lid with the Au-Sn solder reflowed on the Ni/Au metallization. The yellow box indicates an area of incomplete coverage by the Au-Sn solder. (b) High magnification photograph shows the non-wetted Au metallization.



Fig. 8 Photograph shows a lid that had the Au-Sn preform removed to reveal the Ni/Au metallization. The AES analysis was performed at the four locations, A, B, C, and D.

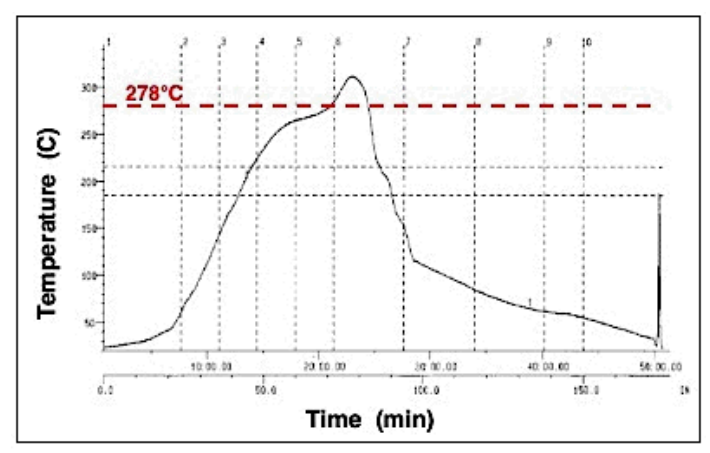


Fig. 9 The time-temperature profile that simulates the supplier Au-Sn reflow process in nitrogen. The melting temperature is 278°C for the Au-Sn solder.

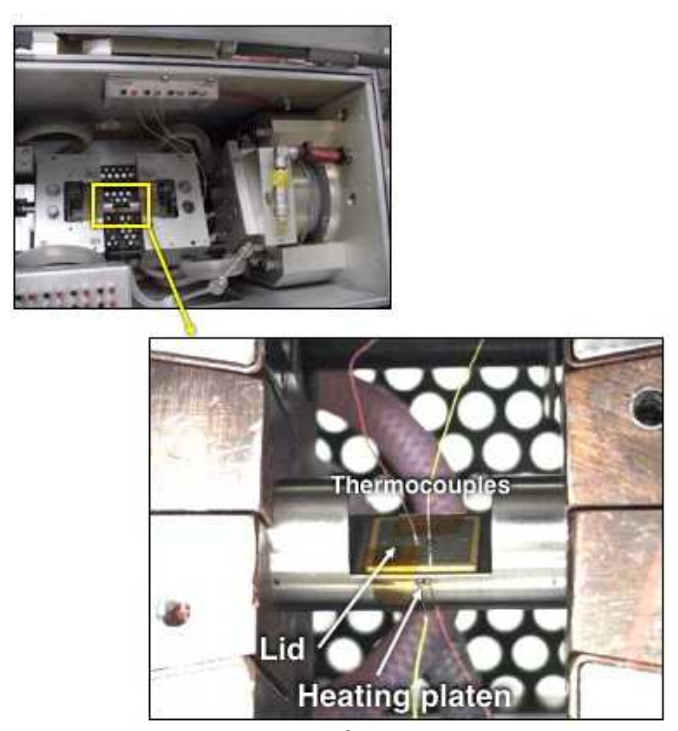


Fig. 10 The upper photograph shows the Gleeble® 3500 equipment used to expose the lid to the batch Au-Sn reflow profile under either a nitrogen or air atmosphere. The lower photograph shows the lid on the heating platen and associated thermal couples to monitor its temperature.

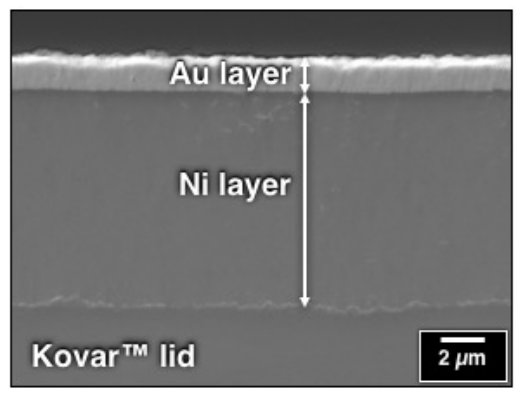
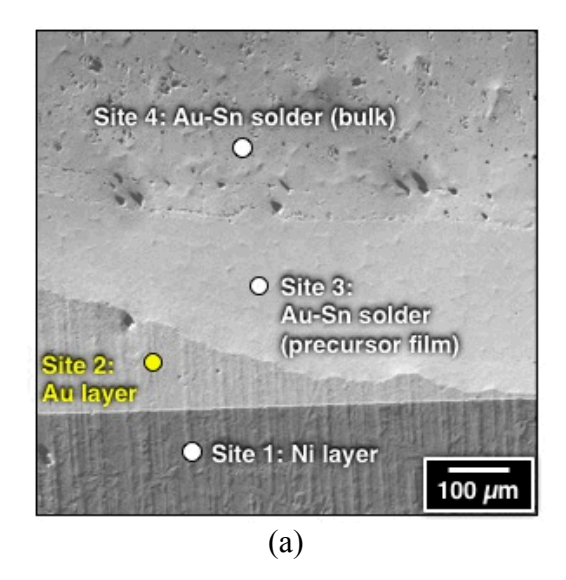


Fig. 11 SEM photograph provides a cross section view of the lid that highlights the Ni and Au layers from which were measured their respective thicknesses.



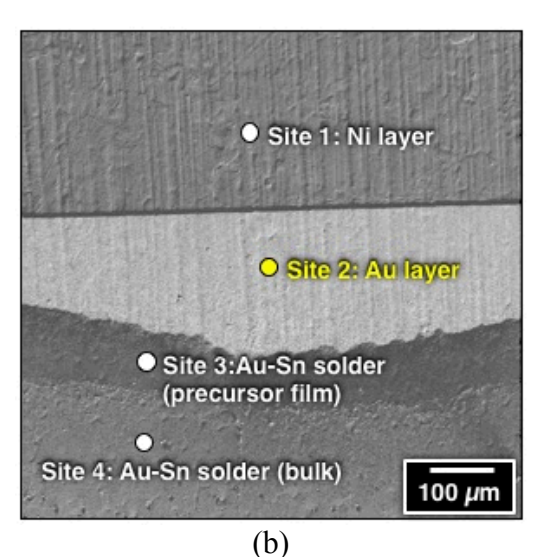
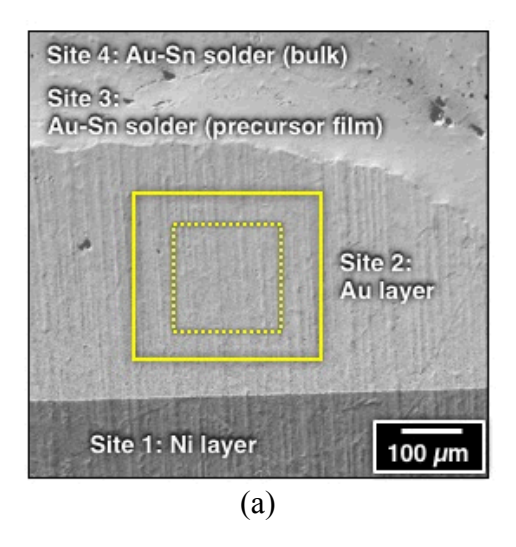


Fig. 12. (a, b) The SEM images show the two locations "A" and "B" where the AES analysis was performed on the lid having the supplier-reflowed, Au-Sn solder. Four sites were examined per location: Site 1, Ni layer that covered the entire lid surface; Site 2, the surface of Au metallization that was not wetted by the Au-Sn solder; Site 3, a precursor film at the edge of the Au-Sn solder; and Site 4, on top of the Au-Sn solder "bulk".



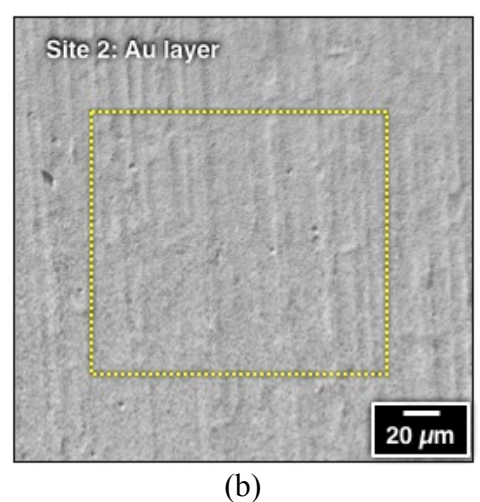


Fig. 13 (a) Low magnification image shows the location of the AES surface survey (solid rectangle) and depth profile (dashed rectangle) performed at a non-wetted area of the Ni/Au metallization on the supplier-reflowed lid. (b) High magnification SEM photograph shows the smooth surface topography at the site of the depth profile.

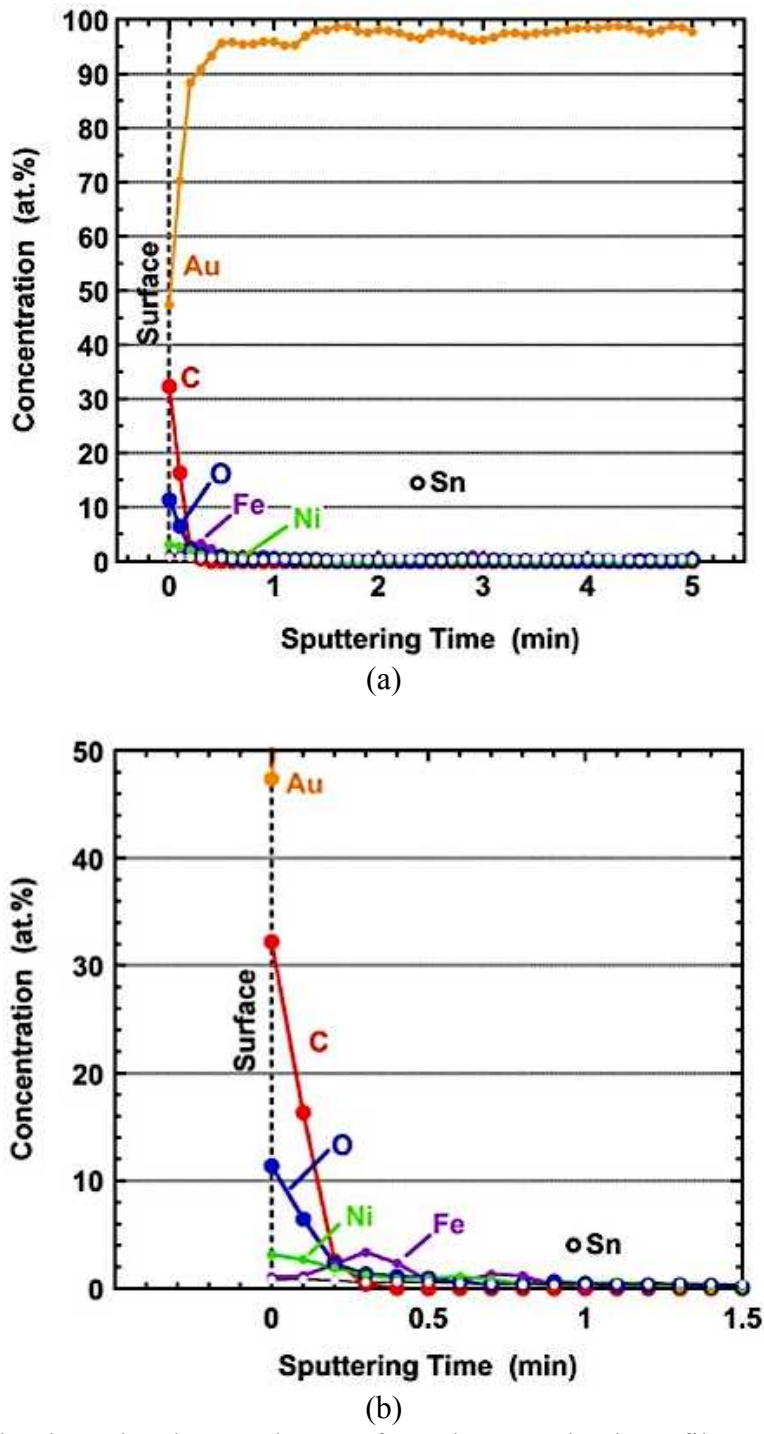


Fig. 14 (a, b) Graphs show the elemental traces from the AES depth profile performed on the non-wetted, Au layer shown in Fig. 13b using two different axes scale.

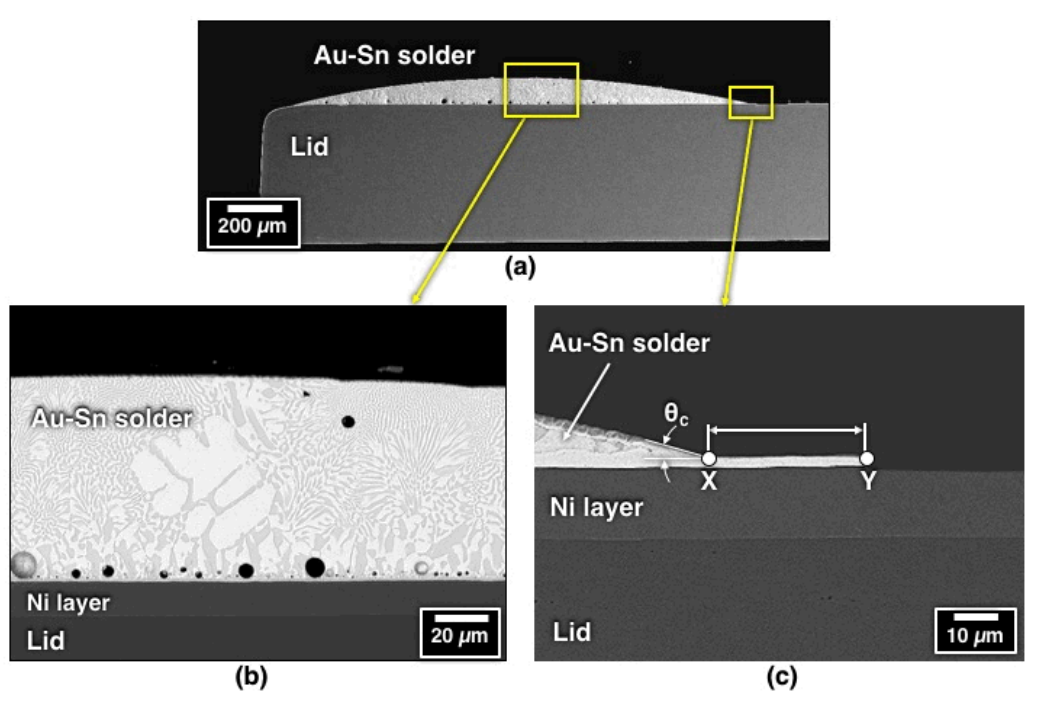


Fig. 15 SEM images show the cross section made through the lid having the Au-Sn solder reflowed on it by the supplier. (a) SEM photograph shows the entire solder coating and locations of the higher magnification images. (b) SEM image shows the Au-Sn solder and its interface with the KovarTM lid at the center location. (c) SEM photograph was taken at the edge of the Au-Sn solder, showing the contact angle, θ_c , and the segment (X-Y) of Au layer that was not covered by the solder.

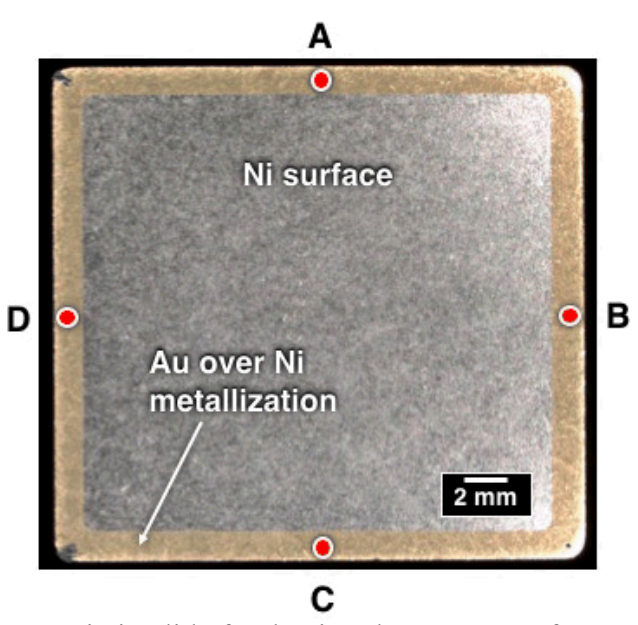


Fig. 16 Photograph shows a pristine lid after having the Au-Sn preform removed from the Au metallization. The AES analyses were performed at the four sites A, B, C, and D.

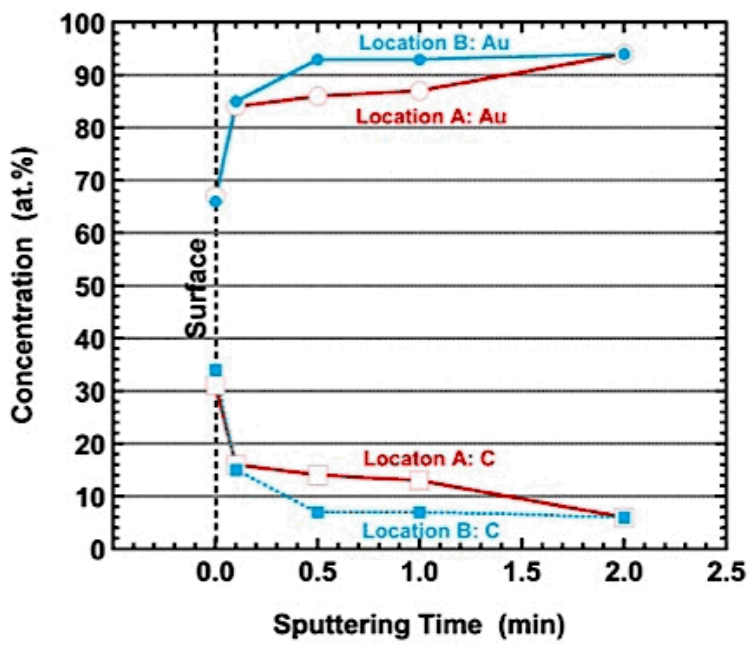


Fig. 17 AES depth profile shows the C and Au signals in the Au metallization of a pristine lid that was not exposed to the Au-Sn solder reflow process. Data are shown for locations A and B; they are representative of results at locations C and D, as well.

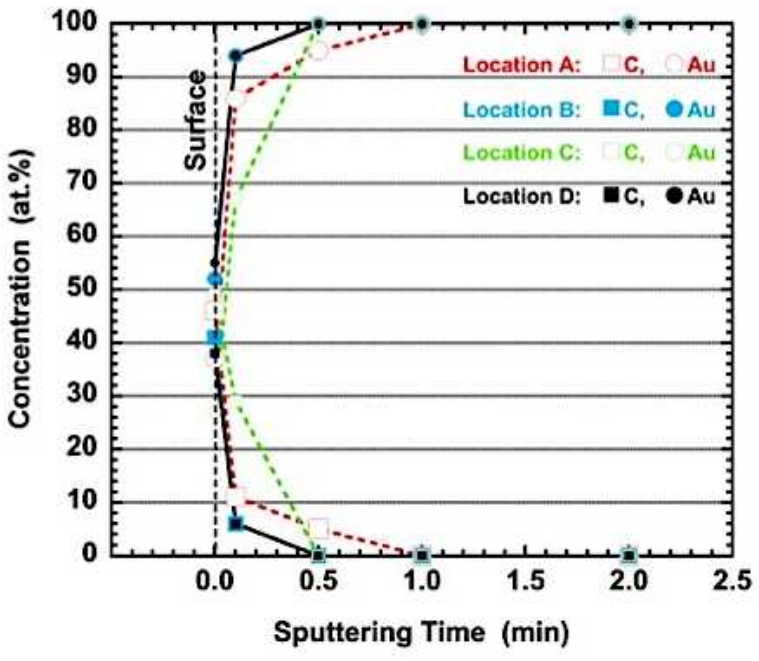


Fig. 18 AES depth profile shows the C and Au signals obtained from the four locations A, B, D, and C on the Au layer of a pristine lid after exposure to the simulated, nitrogen reflow process.

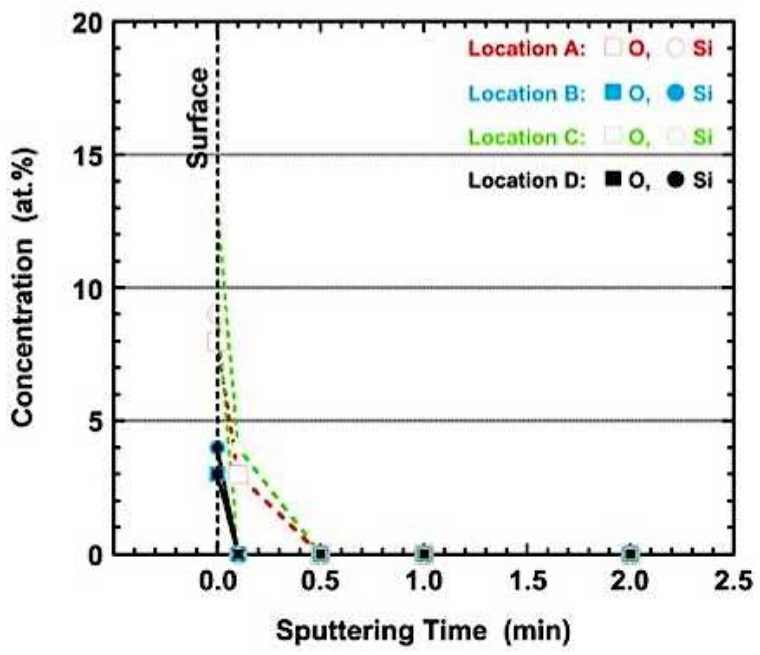


Fig. 19 AES depth profile shows the Si and O signals on the Au metallization following exposure to the nitrogen reflow.

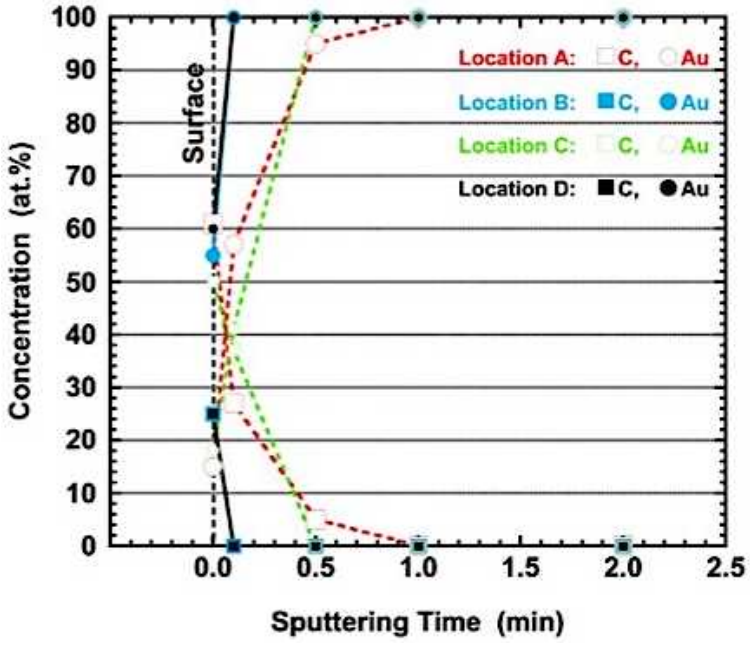


Fig. 20 AES depth profile shows the C and Au signals obtained from the four locations A, B, D, and C on the Au layer of a pristine lid after exposure to the simulated, air reflow process.

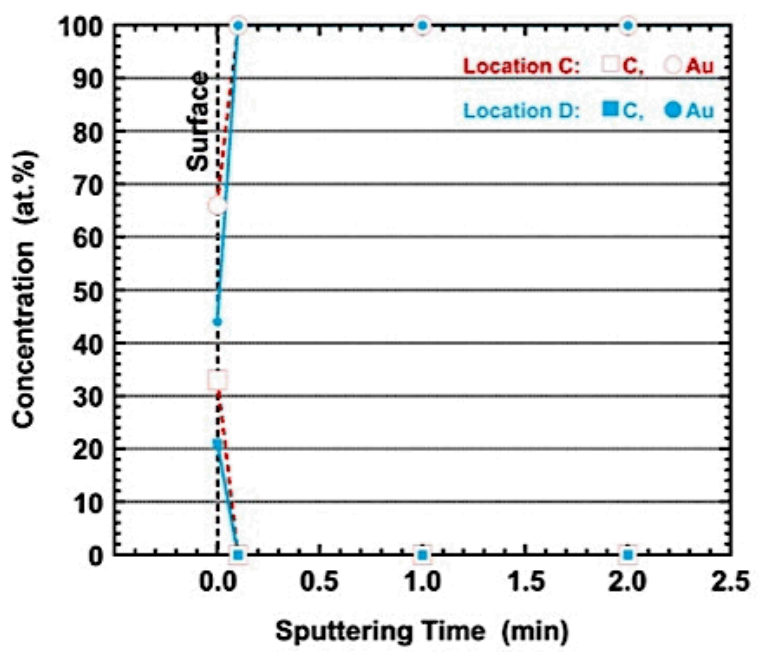


Fig. 21 AES depth profile shows the C and Au signals on the Au layer of the first of three lids. This lid, which had the Au-Sn preformed removed, had *not* been exposed to the belt furnace reflow process.

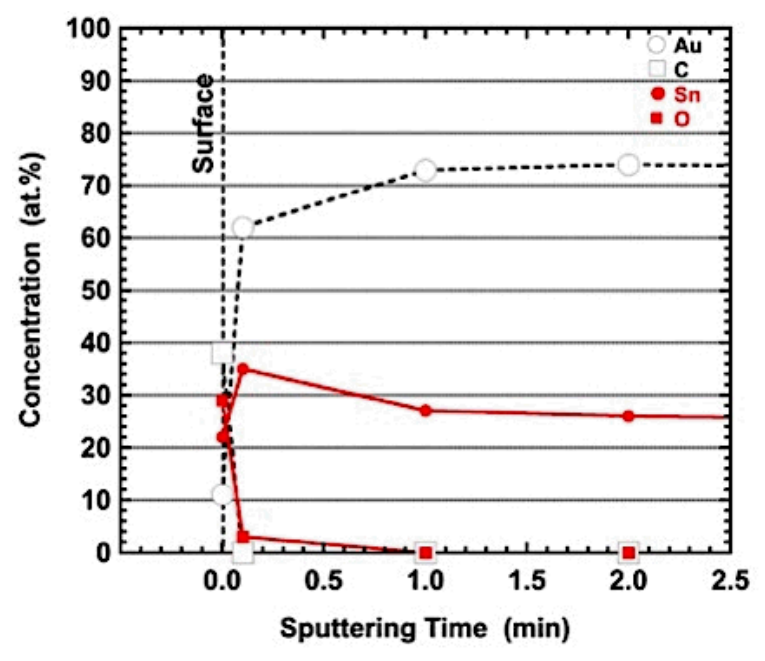


Fig. 22 AES depth profile shows the first 2.5 minutes of a ten-minute depth profile taken on the surface of the Au-Sn preform.

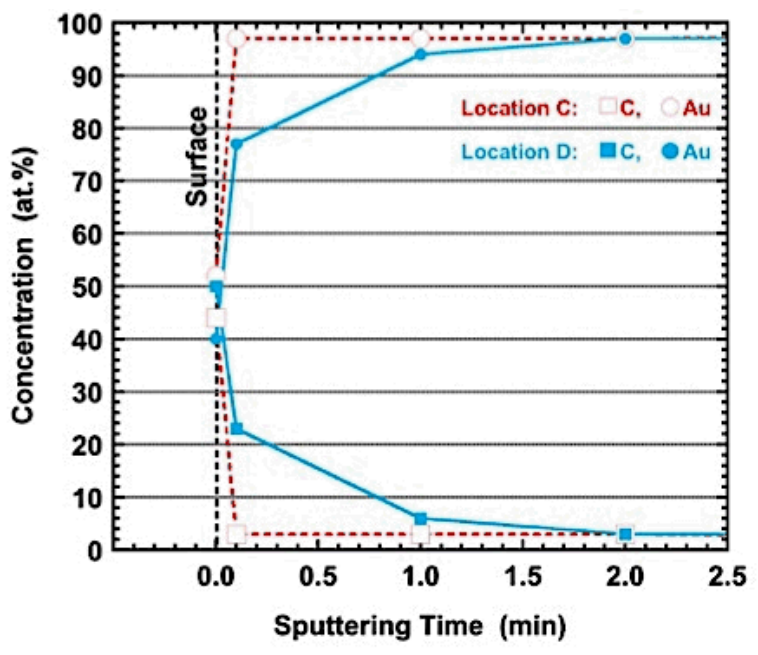


Fig. 23 AES depth profile taken after exposure to the belt furnace reflow process (nitrogen). The sites were just to the side of the those used to obtain the baseline data in Fig. 21.

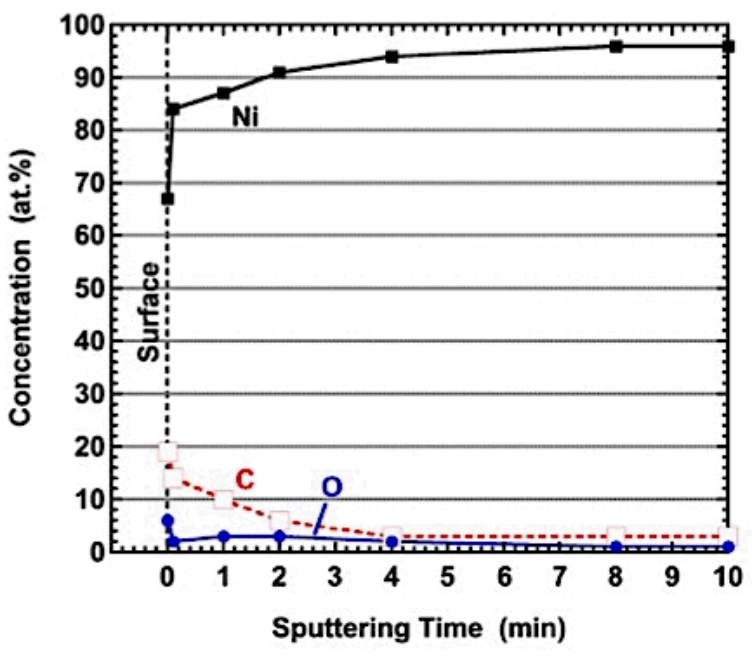


Fig. 24 AES depth profile taken of the Ni at the center of the lid after exposure to the belt furnace reflow process (nitrogen).

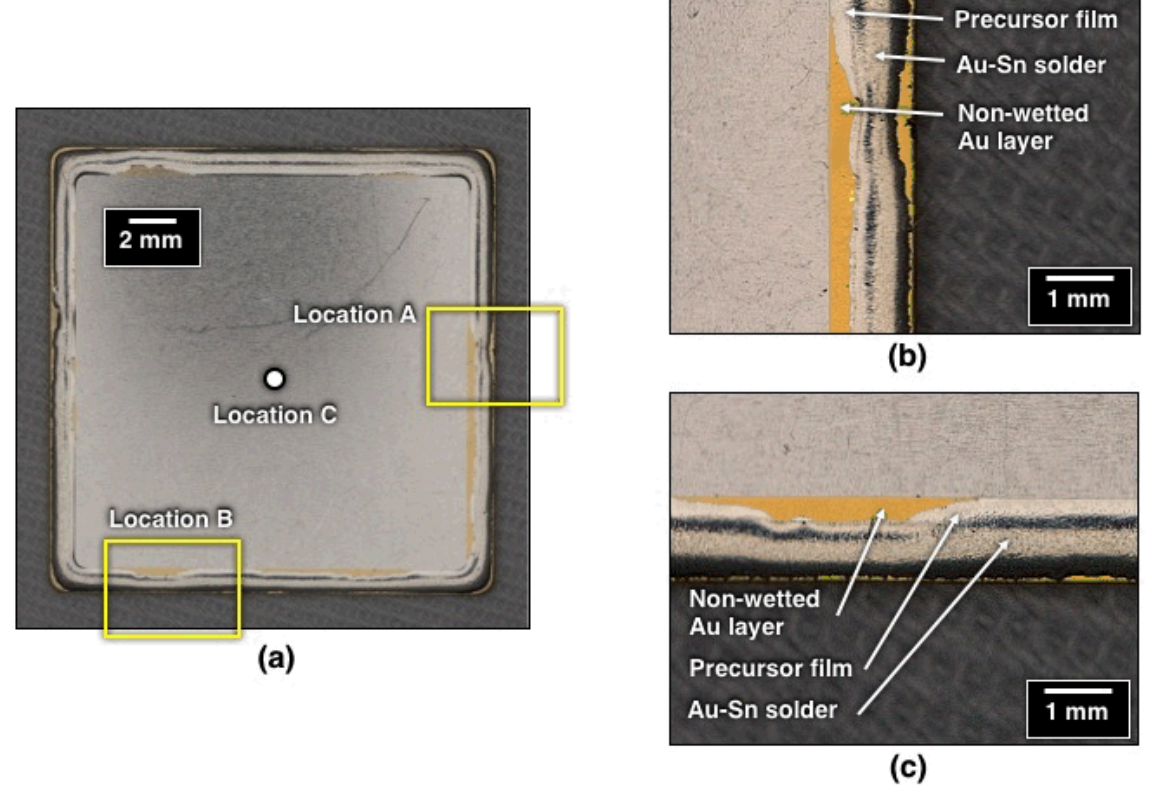


Fig. 25 (a) Photograph shows the second of three lids after exposure to the belt furnace reflow process. Two locations, A and B, are shown at higher magnification in (b) and (c), respectively. The AES analyses were on the non-wetted Au layer; the precursor film (Au-Sn solder); and the Au-Sn solder (mound).

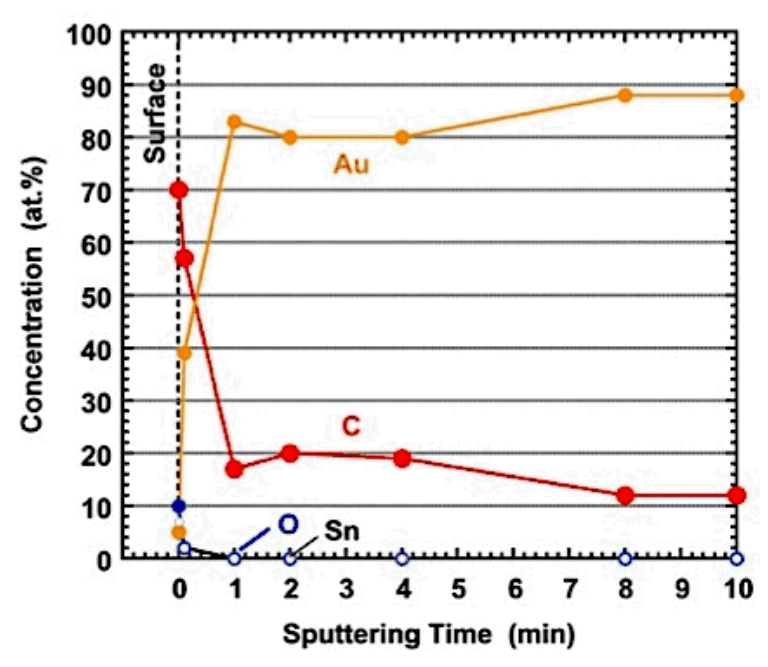


Fig. 26 AES depth profile taken at the non-wetted region of Location A on the second of three lids that was exposed to the belt furnace reflow process.

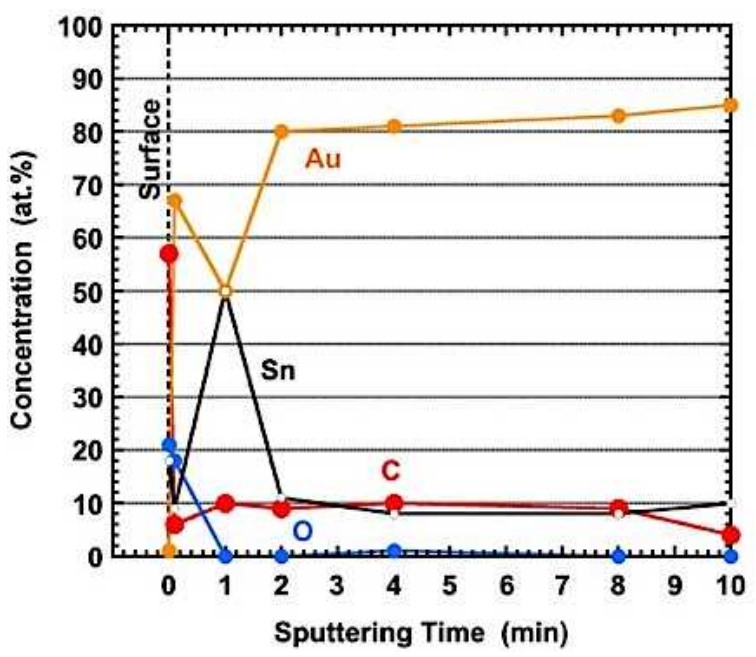


Fig. 27 AES depth profile taken at the precursor film region of Location A on the second of three lids exposed to the belt furnace reflow process.

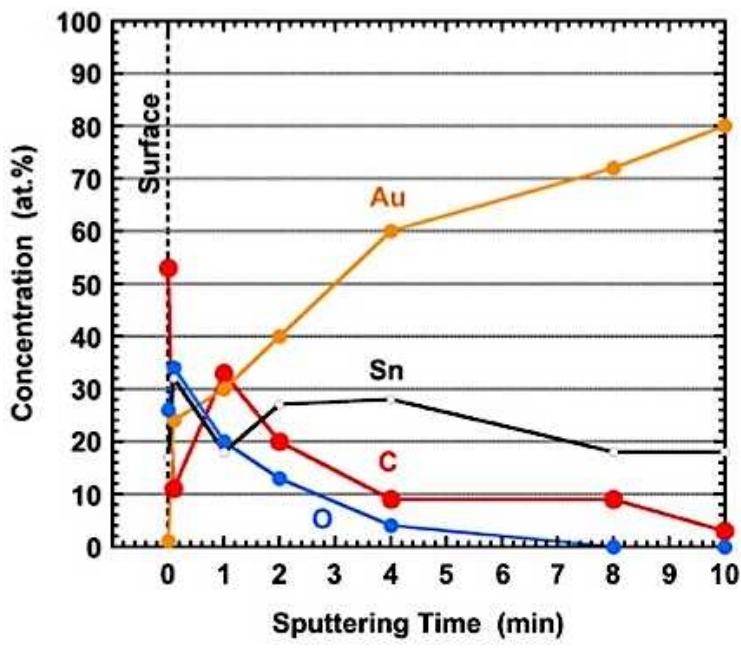
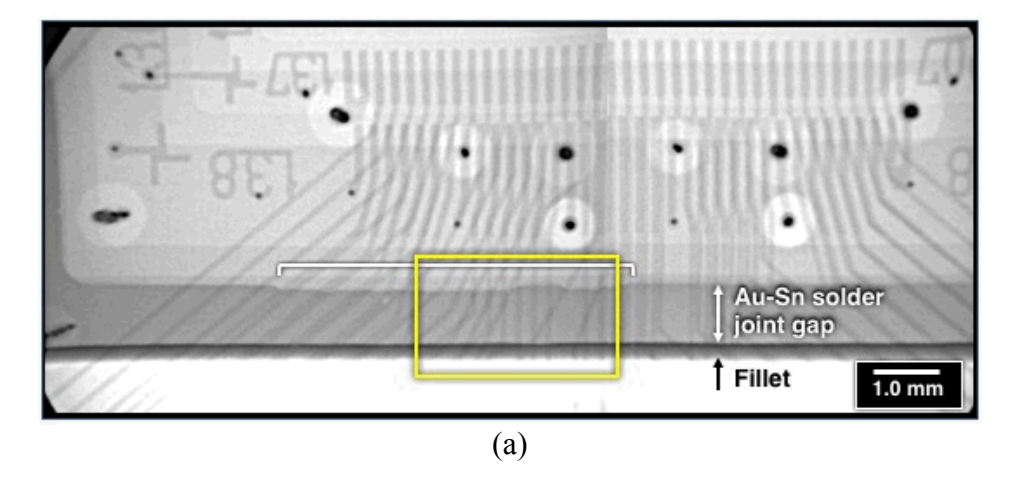


Fig. 28 AES depth profile taken at the bulk Au-Sn solder of Location B on the second of three lids exposed to the belt furnace reflow process.



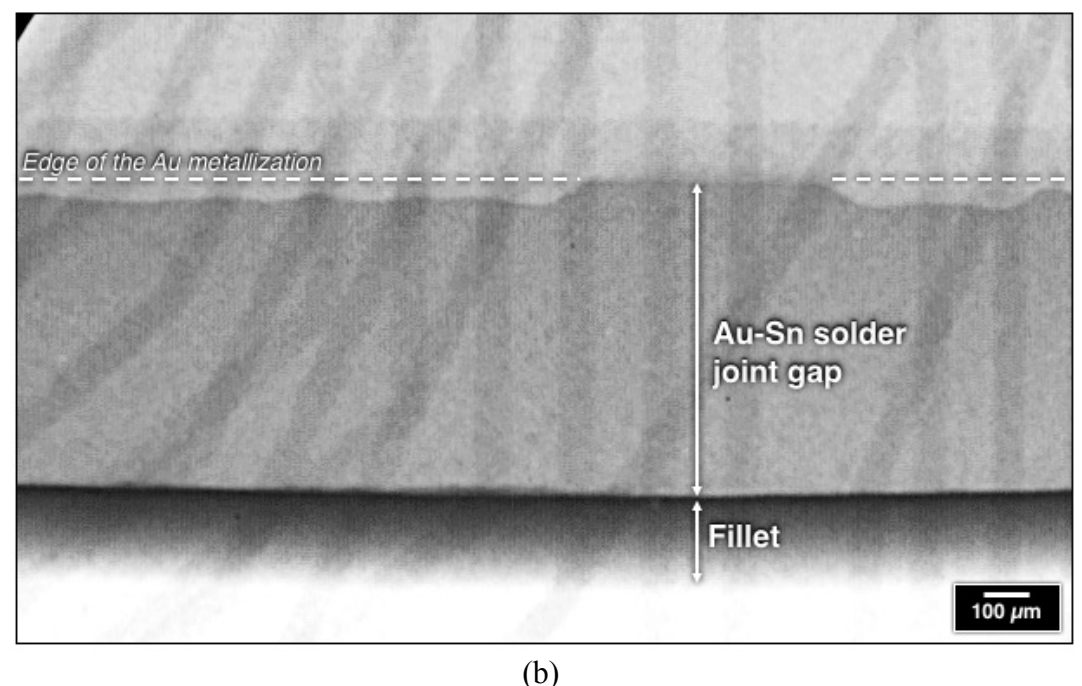


Fig. 29 (a) X-ray radiograph shows a section of the Au-Sn solder joint made between the third lid and ceramic frame. The fillet (outside) and joint gap are identified in the image. The white bracket indicates the (only) location of the joint where the solder did not wet-and-spread completely over the Au layer belonging to the lid. (b) A higher magnification radiograph was taken of the Au-Sn solder joint at the location of the yellow box in image (a). The radiograph illustrates the extent of non-wetting versus the full footprint of the joint identified as the "Au-Sn solder joint gap."

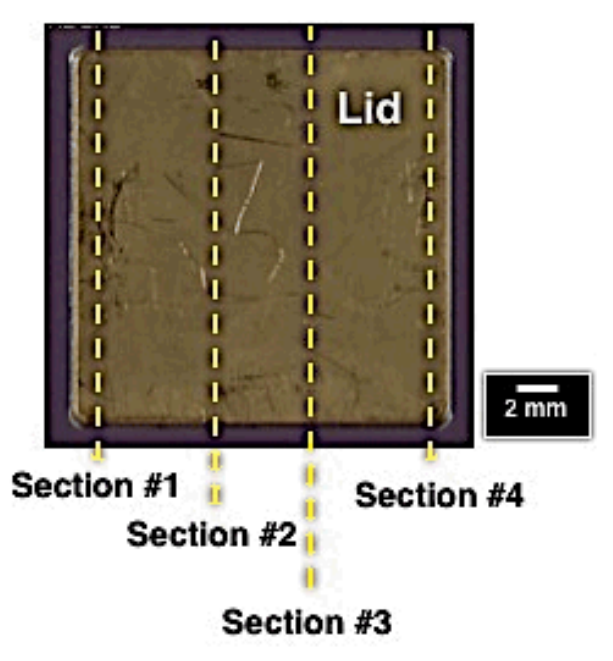


Fig. 30 Photograph shows the locations of the four cross sections made to the Au-Sn solder joint between the third lid and the ceramic frame.

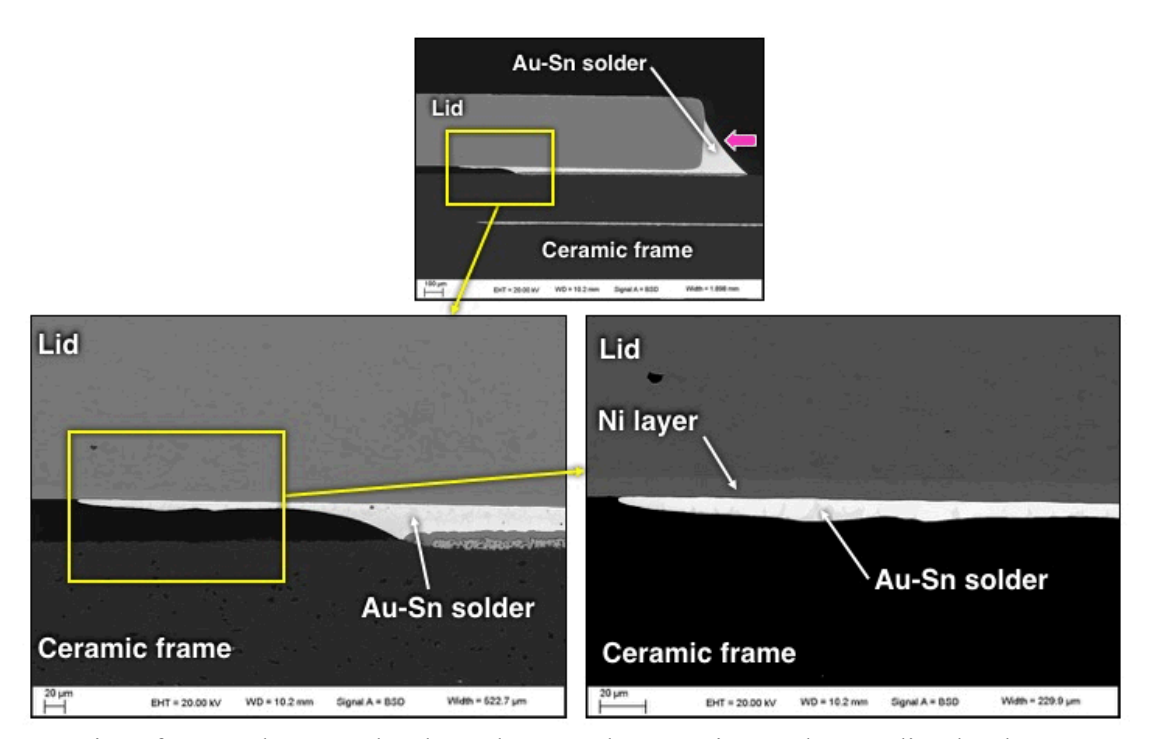


Fig. 31 Series of SEM photographs show the complete wetting-and-spreading by the Au-Sn solder over the Au metallization at section #2. The magenta arrow indicates the excellent fillet formation. The high magnification images confirm that the Au-Sn solder wet and spread to the edge of the lid's metallization.

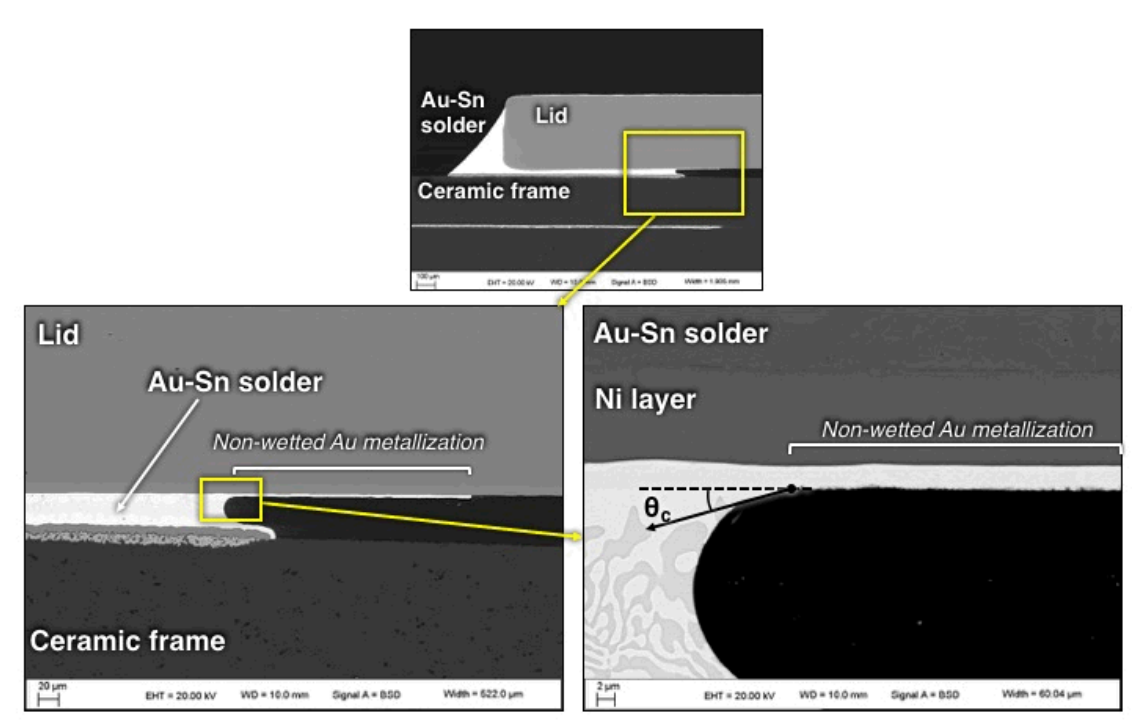


Fig. 32 Series of SEM photographs that exemplify failure of the Au-Sn solder to completely cover the Au metallization at the other side of section #2. The high magnification images confirm the generally good solderability of the Au metallizations on both the lid (low contact angle, θ_c) and ceramic frame.

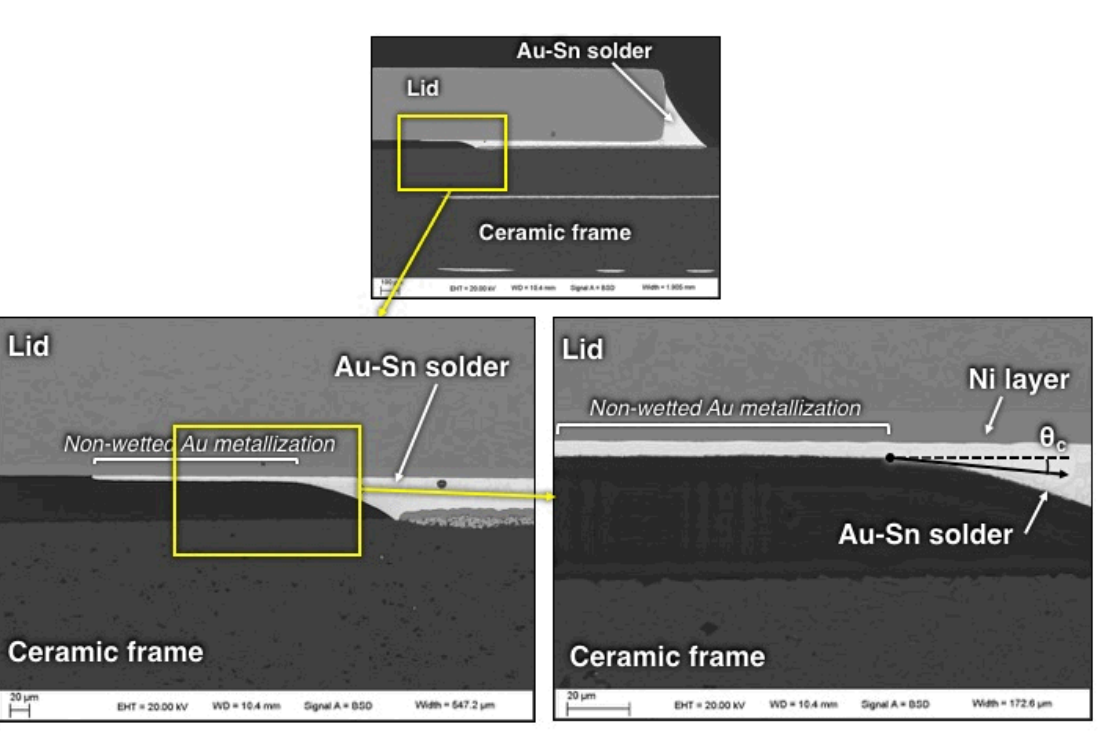


Fig. 33 Series of SEM photographs that show failure of the Au-Sn solder to completely cover the Au metallization at section #3. The geometry of the internal fillet shows a small contact angle, θ_c , that signifies generally good solderability.

Table Titles

D-47930	Element Concentration (at.%)												
Site	С	N	0	Р	s	CI	Ca	Cu	Fe	Co	Ni	Au	Sn
1, Ni layer	35	2	18	1	1	0.5	1	0.1	1	1	37	2	0.5
2, Au layer	45	1	5	0.5	1	0.5	2	0.5	1	2	3	38	1
3, Au-Sn, precursor	50	1	18	0.5	0.5	0.1	1	0.5	1	1	0.5	15	11
4, Au-Sn, bulk	45	1	26	0.5	0.5	ND	1	0.1	1	2	0.5	7	15

Table 1 AES Surface Survey Data Taken at Location A (Fig. 8) on the Lid with Supplier-Reflowed Au-Sn Solder

	Element Concentration (at.%)												
Site	С	N	0	Р	s	CI	Ca	Cu	Fe	Co	Ni	Au	Sn
1, Ni layer	35	2	18	1	2	0.1	2	0.5	1	1	38	2	0.5
2, Au layer	47	1	4	0.5	1	0.1	1	1	0.5	1	2	41	1
3, Au-Sn, precursor	46	1	18	0.5	0.5	ND	1	0.5	2	3	0.5	15	12
4, Au-Sn, bulk	40	3	27	0.5	0.5	ND	1	0.1	2	2	0.5	7	18

Table 2 AES Surface Survey Data Taken at Location B (Fig. 8) on the Lid with Reflowed Au-Sn Solder

05+4100	Element Concentration (at.%)											COST	
Site	С	N	0	Р	S	CI	Ca	Cu	Fe	Co	Ni	Au	Sn
Surface, Large Area	41	1	9	1	1	0.5	2	1	0.5	1	2	41	1
"t=0", Depth Profile Area	32	1	12				2		1		3	48	1

Table 3 AES Surface Survey Data and Results at "t = 0" of the Depth Profile Taken Near Location B (Fig. 8) on Lid with Reflowed Au-Sn Solder

	Element Concentration (at.%)												
Site	С	N	0	Р	S	CI	Ca	Cu	Fe	Co	Ni	Au	Sn
Ni surface	27	1	20	1	2	0.5	3	1	0.5	3	41		1
1 min sputter	6		6							7	81		
1, Ni layer, Loc. 1	35	2	18	1	1	0.5	1	0.1	1	1	37	2	0.5
1, Ni layer, Loc. 2	35	2	18	1	2	0.1	2	0.5	1	1	38	2	0.5

Table 4 AES Surface Survey and Post-One-Minute Sputter Obtained from Locations on the Ni Coating of the Lid with Reflowed Au-Sn Solder

	Elemental Concentrations (at.%)										
Location	С	Au	Ni	Cu							
Α	31	67	1	0.5							
В	34	66	, · · · · · · · ·	2772							
С	30	70	``	12							
D	32	68	1,								

Table 5 AES Surface Surveys Obtained from a "Pristine" Lid.